TITLE

Remodeling of perturbed chromatin can initiate *de novo* transcriptional and post-transcriptional silencing

AUTHORS

Florian Carlier [1,3], Sebastian Castro Ramirez [1,3], Jaafar Kilani [1], Sara Chehboub [1], Isabelle Loïodice [2], Angela Taddei [2], and Eugene Gladyshev [1]*

AFFILIATIONS

[1] Institut Pasteur, Université Paris Cité, Molecular Genetics and Epigenetics Unit, Paris, France

[2] Institut Curie, Université PSL, Sorbonne Université, CNRS, UMR3664 Nuclear Dynamics, Paris, France

[3] Equal contribution

* Correspondence: eugene.gladyshev@gmail.com

ABSTRACT

In eukaryotes, repetitive DNA can become silenced *de novo*, either transcriptionally or post-transcriptionally, by processes independent of strong sequence-specific cues. The mechanistic nature of such processes remains poorly understood. We found that in the fungus *Neurospora crassa*, *de novo* initiation of both transcriptional and post-transcriptional silencing was linked to perturbed chromatin, which was produced experimentally by the aberrant activity of transcription factors at the *tetO* operator array. Transcriptional silencing was mediated by canonical constitutive heterochromatin. On the other hand, post-transcriptional silencing resembled repeat-induced quelling but occurred normally when homologous recombination was inactivated. All silencing of the *tetO* array was dependent on SAD-6 (a fungal ortholog of the SWI/SNF chromatin remodeler ATRX), which was required to maintain nucleosome occupancy at the perturbed locus. In addition, we found that two other types of sequences (the *lacO* array and native AT-rich DNA) could also undergo recombination-independent quelling associated with perturbed chromatin. These results suggested a model in which the *de novo* initiation of transcriptional and post-transcriptional silencing is coupled to the remodeling of perturbed chromatin.

KEYWORDS

Transcriptional gene silencing; post-transcriptional gene silencing; repeat-induced gene silencing; quelling; constitutive heterochromatin; nucleosome-depleted regions; chromatin remodeling; operator arrays; AT-rich DNA; TetR; GATA factors; ATRX; SAD-6; *Neurospora*

CLASSIFICATION

Biological Sciences/Genetics

SIGNIFICANCE STATEMENT

This study addresses an enigmatic question of how transcriptional and post-transcriptional gene silencing can be initiated *de novo* in the absence of strong sequence-specific cues. Using the fungus *Neurospora crassa* as a model organism, we found that both types of silencing can be triggered in mitotic cells by the remodeling of a transiently perturbed (nucleosome-depleted) chromatin state. In this system, the initiation of silencing requires SAD-6, a conserved SWI/SNF chromatin remodeler orthologous to ATRX that has been already implicated in repetitive DNA silencing in fungi, plants, and animals. Thus, the model proposed in this study may underpin a range of gene-silencing phenomena observed in other eukaryotes.

INTRODUCTION

The genomes of most eukaryotes contain large amounts of repetitive DNA silenced transcriptionally and post-transcriptionally by diverse processes. While some of these processes are directed by strong sequence-specific signals (for example, KRAB domain-containing zinc finger proteins recruiting the methyltransferase SETDB1 [1]), others might be induced by the combined effect of multiple weaker interactions, necessitating a threshold number of tandem repeats to initiate silencing [2,3]. This principle may also apply to gene arrays (such as the human D4Z4 array carrying multiple copies of *DUX4* [4]) and transgenic repeats, as documented in fungi [5], plants [6], and animals [7,8]. Notably, in mammals, a screen for regulators of transgenic repeat-induced gene silencing (RIGS) identified a number of factors also required for transcriptional (heterochromatin-mediated) silencing of the native gene arrays [9,10], suggesting that the underlying mechanisms could be conserved.

ATRX (Alpha Thalassemia/Mental Retardation Syndrome X-Linked) is a member of the SWI/SNF family of chromatin remodelers [11]. In a complex with the histone chaperone DAXX, ATRX was shown to deposit the histone variant H3.3 at several types of repetitive sequences (pericentromeric, telomeric, ribosomal and other repeats) as well as non-repetitive regions [11]. H3.3 deposited by ATRX-DAXX often carries H3K9me3 [11]. Overall, ATRX has roles in several chromatin-based processes including transcriptional silencing of repetitive DNA, telomere maintenance, resolution of secondary DNA structures, and regulation of gene expression [11]. In addition to DAXX, ATRX is known to interact with other chromatin factors (proteins and long noncoding RNAs) as well as specific histone modifications (H3K9me3 and H3K4me0) [11]. ATRX is also known for its ability to recognize and remodel nucleosome-depleted chromatin linked to aberrant transcription, such as the Hsp70 genes during heat shock in Drosophila [12] and GC-rich telomeric repeats giving rise to R-loops [13].

The fungus *Neurospora crassa* sports several genome-defense processes that involve the *de novo* initiation of transcriptional and post-transcriptional silencing. First, in vegetative cells of *N. crassa*, transgenic repeats can become heavily methylated, as the result of potent RIGS [5]. Second, during sexual reproduction, duplications of genomic DNA longer than a few hundred base-pairs trigger repeat-induced point mutation (RIP), by which many cytosines in repeats are converted to thymines [14,15]. Interestingly, RIP can be carried out by the same pathway that establishes *de novo* DNA methylation during RIGS [5,16].

Concerning the initiation of post-transcriptional silencing, two processes need to be considered. One process, known as quelling, triggers the expression of small interfering RNAs (siRNAs) from repetitive transgenes in vegetative cells [17]. Another process, known as meiotic silencing by unpaired DNA (MSUD), takes place in early meiosis and induces the expression of siRNAs from the mismatching loci found at the allelic positions on pairs of homologous chromosomes [18,19]. Whereas MSUD occurs normally without DNA breakage and

recombination [20], quelling was proposed to rely on recombinational DNA repair as a mechanism for repeat recognition [21]. Interestingly, potent MSUD was shown to require SAD-6, a fungal ortholog of ATRX [22].

A substantial part of the *N. crassa* genome corresponds to AT-rich DNA (produced by RIP), which nucleates H3K9me3 through a process mediated by the SUV39 methyltransferase DIM-5 [23]. In its turn, H3K9me3 is recognized by HP1 (Heterochromatin Protein 1), which forms a complex with the cytosine methyltransferase DIM-2 responsible for all DNA methylation in this organism [23]. Thus, in *N. crassa*, AT-rich DNA functions as a hard-wired signal for the formation of constitutive heterochromatin and ensuing DNA methylation [23]. Several additional components of this pathway were identified, including histone deacetylases and chromatin remodelers [24,25]. In parallel, a more dynamic type of DNA methylation occurs at some loci associated with antisense transcription [26,27]. Interestingly, this DNA methylation also requires DIM-5 and HP1 [28].

This study was motivated by two earlier results. First, in *N. crassa*, a long *tetO* operator array was reported to trigger RIP by the heterochromatin-related pathway, suggesting that it could initiate transcriptional silencing [29]. Second, in budding yeast, the association of such arrays with their corresponding repressor proteins was shown to induce transcriptional silencing of a nearby gene [30,31]. That process started with phosphorylation and concomitant depletion of histone H2A, suggesting that the binding of repressor proteins led to chromatin stress and nucleosome loss; and it did so by a mechanism independent of DNA replication [30]. The perturbed array was directed to the perinuclear compartment, where it became occupied by Silent Information Regulator (SIR) proteins, the main effectors of heterochromatic silencing in yeast [30]. Overall, it was proposed that the tight yet dynamic binding of repressor proteins could accelerate the turnover of nucleosomes and promote the incorporation of histones without certain modifications (such as H3K79me3), which would normally interfere with the recruitment of SIR proteins [30].

We now report that the *lacO* and the *tetO* operator arrays [32], when integrated as single-copy constructs and never exposed to RIP, can initiate strong transcriptional and post-transcriptional silencing in somatic cells of *N. crassa*. At the *tetO* array, the silencing was induced by the aberrant activities of either TetR-GFP or NIT-2 (a transcription factor of the GATA family). Both situations were associated with locally perturbed chromatin. Transcriptional silencing of this locus was mediated by canonical constitutive heterochromatin. On the other hand, post-transcriptional silencing resembled quelling but still occurred normally in the absence of RAD51 or RAD52, two main recombination factors. Therefore, this process was named recombination-independent quelling (RIQ). All silencing of the *tetO* array was dependent on SAD-6 (a fungal ortholog of the SWI/SNF chromatin remodeler ATRX), which was required to maintain nucleosome occupancy at the perturbed locus. In addition, we found that two other types of sequences (the *lacO* array and native AT-rich DNA) could also undergo recombination-independent quelling associated with perturbed chromatin. These results suggested a

model in which the *de novo* initiation of transcriptional and post-transcriptional silencing is coupled to the remodeling of perturbed chromatin.

RESULTS

Experimental system

In budding yeast, the binding of bacterial repressor proteins to their corresponding operator arrays can trigger transcriptional silencing of a nearby reporter gene [31]. It was interesting to test if a similar process occurred in *N. crassa*, an organism with canonical transcriptional (heterochromatin-mediated) and post-transcriptional (RNAi-mediated) silencing [23]. To this end, the standard *lacO* and *tetO* arrays were used [32]. These arrays contained 168 *lacO1* and 191 *tetO* sites (interspersed with random sequences), and were characterized by GC-content of ~40% and ~50%, respectively (Fig. S1A). In addition, the *lacO* array included three perfect repeats of several hundred base-pairs (Fig. S1A). The arrays were concatenated on a plasmid and integrated between *his-3* and *lpl* by homologous recombination (Fig. 1A: 'Strain A'). A synthetic construct expressing TetR-GFP was subsequently integrated as the replacement of *csr-1+* (Fig. 1A: 'Strain B'). To protect the arrays from RIP and to eliminate the effects of cytosine methylation on H3K9me3 [23], the genes encoding DIM-2 and RID (a putative cytosine methyltransferase involved in RIP) were deleted in all strains used in this study. The state of chromatin was assayed by ChIP-seq and MNase-seq, while expression of small RNAs (sRNAs) was followed by sRNA-seq.

Binding of TetR-GFP to the *tetO* array induces strong transcriptional and post-transcriptional silencing

In the absence of TetR-GFP (in Strain A), only very low levels of sRNAs were expressed from the arrays (Fig. 1E,F; Fig. S1B). Interestingly, the *lacO* array was strongly enriched in H3K9me3 (Fig. 1D). An AT-rich motif 'ATAACAATT' was noted in the sequence of *lacO1* (Fig. S1A), raising a possibility that the *lacO* array could nucleate heterochromatin analogously to native AT-rich DNA in *N. crassa* [23].

Two remarkable results were observed at the *tetO* array in the presence of TetR-GFP. First, the array appeared strongly heterochromatic (Fig. 1D: 'Strain B'). Second, it also started to express very large amounts of sRNAs (Fig. 1E,F: 'Strain B'). These sRNAs were predominantly 20-23 nt long and had a strong bias for uracil at the 5' position (Fig. 1B). Both processes were suppressed by tetracycline (Fig. 1D,E: 'Strain B + Tc'), implicating the binding of TetR-GFP as a causative trigger of all silencing in this system.

Interestingly, the binding of TetR-GFP to the *tetO* array also stimulated sRNA expression at several loci as far as 100 kbp away from the array (Fig. S1B). The majority of those loci were non-coding. Such a long-distance

effect may involve global repositioning of the array-carrying chromosomal segment, as reported previously in budding yeast [30], or increasing concentration of some critical RNAi factor in the vicinity of the array [33].

A set of endogenous sRNA loci provides a standard reference for comparative sRNA-seq analysis

To compare expression of array-derived sRNAs between different conditions, a set of endogenous sRNA loci was selected as a standard reference. Such loci were chosen for their strong and invariant expression patterns, mostly corresponding to tRNA and 5S RNA genes (several examples are shown in Fig. S1C). For the purpose of this analysis, those loci were represented by 463 non-overlapping 500-bp tiles (SI Data File 3). For a given condition, the reference level was calculated as the median number of sRNA-seq reads mapped to those tiles. This value was used to normalize the levels of array-derived sRNAs calculated as the median number of reads mapped to the 500-bp tiles overlapping the arrays. Notably, this method could also be used to compare sRNA expression between *Neurospora* strains of different genetic origin (Fig. S1D).

The *lacO–tetO* locus undergoes recombination-independent quelling (RIQ)

In *Neurospora*, expression of sRNAs from transgenic repeats represents a hallmark of quelling [17]. Thus, we asked if *tetO*-derived sRNAs required quelling factors QDE-1 (an RNA-dependent RNA polymerase), QDE-2 (an Argonaute protein), and QDE-3 (a RecQ helicase). The loss of QDE-1 suppressed *tetO*-derived sRNAs to the background levels corresponding to the repressor-free condition (Fig. 1C,F). The loss of QDE-3 produced a similar result, yet some residual expression of *tetO*-derived sRNAs above background could still be detected (Fig. 1C,F). In both conditions, the *tetO* array remained occupied by TetR-GFP (Fig. S2B). On the other hand, *tetO*-derived sRNAs did not require QDE-2, consistent with the fact that QDE-2 was dispensable for making sRNA during quelling (Fig. 1C,F). The levels of *lacO*-derived sRNAs, although being lower by two orders of magnitude compared to *tetO*-derived sRNAs, exhibited similar regulatory patterns (Fig. 1C,F).

We also tested the role of ERI1, a conserved exonuclease implicated in heterochromatin assembly and sRNA production associated with antisense transcription in *N. crassa* [34]. We found that ERI1 was not required for the expression of array-derived sRNAs in our system (Fig. 1C,F).

Earlier studies in *N. crassa* linked quelling with homologous recombination [21]. Thus, we asked if the newly uncovered quelling-like process required RAD51 and RAD52, the two critical recombination factors. Several effects were observed in the corresponding gene-deletion strains. First, the expression of *tetO*-derived sRNAs was not affected by the loss of RAD51 or RAD52 (Fig. 1C,F). Second, the expression of subtelomeric sRNAs became upregulated (Fig. 1F; Fig. S3C). Third, the proportion of background sRNAs (produced at low levels throughout the genome [35]) became strongly elevated as well (Fig. 1F; Fig. S3C). The loss of RAD52 had a greater impact compared to the loss of RAD51.

In *N. crassa*, the expression of some sRNA types requires the acetyltransferase RTT109 [36], which catalyses acetylation of H3K56 to control nucleosome dynamics coupled to DNA replication and repair [37]. We found that the loss of RTT109 had a strong impact on *tetO*-derived sRNAs, reducing their levels 52-fold (Fig. 1C,F). Interestingly, in this condition, the genome-wide pattern of sRNA expression resembled those observed in the absence of RAD51 or RAD52 (Fig. 1F; Fig. S3C). These results corroborated the previously reported role of RTT109 in sRNA biogenesis in *N. crassa* [36] and hinted at a possibility that RTT109 exerted its specific role in the production of *tetO*-derived sRNAs by modulating nucleosome homeostasis linked to DNA replication, rather than recombinational DNA repair.

Taken together, these results supported two conclusions. First, in *Neurospora*, similarly to budding yeast [31], the repressor-bound *tetO* array was engaged in transcriptional (heterochromatin-mediated) silencing. Second, the same locus was also engaged in post-transcriptional (RNAi-mediated) silencing, which resembled repeat-induced quelling but still occurred normally when homologous recombination was disabled. This process was named recombination-independent quelling (RIQ).

Type I topoisomerase TOP3 is dispensable for RIQ

Sgs1 (the yeast ortholog of QDE-3) partners with the type I topoisomerase Top3 to form a conserved complex involved in recombinational DNA repair [38]. Thus, we asked if a *Neurospora* ortholog of Top3 played a role in RIQ. We found that the *top3Δ* condition was associated with a 6-fold decrease in *tetO*-derived sRNAs and a 10-fold increase in *lacO*-derived sRNAs (Fig. 1C,F). An elevated proportion of background sRNAs was noted as well (Fig. 1F). The latter effect is exemplified by having many sRNA-seq reads mapped to the active genes near the *lacO–tetO* locus (Fig. S3B). These results suggested that QDE-3 mediated RIQ by a mechanism that did not require TOP3.

Heterochromatin assembly during RIQ is both RNAi- and recombination-independent

Our ChIP-seq analysis yielded several insights. First, the bulk levels of histone H3 at the *tetO* array decreased in the presence of TetR-GFP, indicating the occurrence of stressed (perturbed) chromatin (Fig. S2C). Second, the arrays remained perfectly heterochromatic when QDE-1, QDE-2, QDE-3, ERI1, RAD51, or RAD52 were removed individually (Fig. S2A,D), supporting the idea that, in *Neurospora*, constitutive heterochromatin and RNAi were largely independent from one another.

Interestingly, we found that the repressor-bound *tetO* array had its H3K9me3 levels decreased in the absence of RTT109 (Fig. S2A,D). This effect was not associated with apparent changes in the hH3 occupancy (relative to the parental strain), implying that TetR-GFP was still present normally (Fig. S2A,C). We used fluorescence

microscopy as an independent approach to confirm this conclusion (Fig. S4). We note that the role of RTT109 in constitutive heterochromatin assembly was reported earlier in fission yeast [39].

RIQ is constrained by constitutive heterochromatin

We next asked if the expression of array-derived sRNAs was constrained by constitutive heterochromatin. We found that the *lacO–tetO* locus lost all H3K9me3 in the absence of the histone deacetylase HDA1 (Fig. S2A). This process was linked to a decrease in the hH3 levels at the *lacO* array (Fig. S2C); and a comparable loss of hH3 also occurred at AT-rich DNA (Fig. S2C). With respect to sRNAs, two effects were observed. First, in the *hda1Δ* condition, the expression of *tetO*- and *lacO*-derived sRNAs surged 18- and 539-fold, respectively (Fig. 1C,F). Second, large amounts of sRNAs also became expressed from many AT-rich regions across the genome (Fig. 1F; Fig. S3A,C). A similar pattern was reported earlier in *Neurospora* strains lacking all heterochromatin [40].

SAD-6 controls all silencing of the repressor-bound *tetO* array

An emerging connection between perturbed chromatin and RIQ encouraged us to investigate the involvement of chromatin remodeling factors. We started by testing CHD1 (Chromodomain Helicase DNA Binding Protein 1), which was already implicated in transcriptional and post-transcriptional silencing in *N. crassa* [21,26]. We found that the loss of CHD1 had no impact on the levels of hH3 or H3K9me3 at the arrays (Fig. S5A,C,D). To a first approximation, the levels of array-derived sRNAs were not affected as well (Fig. S5B).

Our results indicated that RIQ resembled MSUD in being recombination-independent. Therefore, we asked if the SWI/SNF chromatin remodeler SAD-6, which belongs to the ATRX clade and represents a critical MSUD factor [22], was involved in RIQ. Several surprising results were observed in the *sad-6Δ* condition. First, the expression of *tetO*-derived sRNAs decreased to a very low level associated with the absence of TetR-GFP and QDE-1 (Fig. 2A; Fig. S6A). We confirmed (by ChIP-seq and microscopy) that TetR-GFP was still present at the *tetO* array in this situation (Fig. 2B; Fig. S4). Second, the *tetO* array was no longer enriched in H3K9me3 (Fig. 2B). Third, the loss of silencing was accompanied by a strong decrease in the hH3 occupancy over DNA containing the *tetO* sites (Fig. 2B). Notably, hH3 was still retained at the *GmR* gene (in the middle of the *tetO* array); however, it was not associated with H3K9me3 (Fig. 2B). Fourth, the hH3 occupancy was restored in the presence of tetracycline (Fig. 2B). Fifth, similar dynamics was also exhibited by histone H2B (Fig. 2D).

The coordinated depletion of hH2B and hH3 (both encoded by single-copy genes in *N. crassa* [23]) pointed to the loss of entire nucleosomes. However, such an effect could also result from changes in epitope accessibility for ChIP. We used MNase sensitivity profiling to discriminate between these two possibilities. To this end, we found that the *tetO* array became progressively sensitive to MNase as its histone ChIP-seq coverage decreased

(Fig. 2C,E; Fig. S2C), implying that the latter served as a reliable measure of nucleosome occupancy. Overall, the unperturbed *tetO* array was characterized by low and largely uniform MNase sensitivity (Fig. S7A: 'Strain A'). Upon binding the repressor, the sensitivity of the array increased but still remained largely uniform (Fig. S7A: 'Strain B'). This uniformity was disrupted in the absence of SAD-6 (Fig. S7A: *sad-6Δ*). Corresponding hH2B/hH3 ChIP-seq profiles hinted at a possibility that some strongly protected sites in the *sad-6Δ* condition could still feature nucleosomes in a fraction of the nuclei (Fig. S7B).

Genome-wide comparison of the *sad-6+*/*sad-6Δ* conditions yielded several results. First, the strong depletion of hH2B and hH3 in the *sad-6Δ* condition was restricted to the *tetO* array and rDNA (Fig. S6B,F). The latter result was intriguing, but it was not pursued in this study. Our further analysis revealed that the *tetO* array was the only genomic region incorporating more than 6 consecutive 500-bp 'strongly nucleosome-depleted' (SND) tiles (defined by having the log10-transformed (IP[hH3]+1)/(Input+1) ratio of -0.5 or less; Fig. 2E,F). Second, besides the *tetO* array, and possibly rDNA, constitutive heterochromatin was lost at only one additional locus, designated as '*r2*' (Fig. S6B,F,J). Third, only one other unrelated locus, designated as '*r1*', had its sRNA levels reduced in the absence of SAD-6 (Fig. S6E,I). In the wildtype, this region produced sRNAs from both strands by a process that also required QDE-1 (Fig. S3C; Fig. S6I). Fourth, the *tetO* array was the only genomic locus characterized by such a dramatic increase in MNase sensitivity (Fig. S6C,G).

SAD-6 is specifically recruited to the repressor-bound *tetO* array

To test if SAD-6 regulated the *tetO* array directly, we replaced the promoter of the native *sad-6+* gene with a construct that (i) provided an N-terminal 3xFLAG tag and (ii) increased the expression of the tagged SAD-6 protein to compensate for a partial loss of its activity (Fig. S6D). We found that tagged SAD-6 became highly and specifically enriched at the repressor-bound *tetO* array, where it was partially active (as evidenced by the intermediate levels of hH3 and H3K9me3 at the array, Fig. 2G). Genome-wide, comparable enrichment was only observed at one additional locus (designated as '*r3*'), which overlapped the promoter of NCU01783 (Fig. S6H,K). The latter effect was unexpected yet reproducible (Fig. S6K). Taken together, these results suggested that the repressor-bound *tetO* array represented a particularly favorable substrate for SAD-6.

NIT-2 is required for the *de novo* silencing of the *tetO* array induced by nitrogen starvation

Our results demonstrated that aberrant binding of TetR-GFP perturbed chromatin and initiated transcriptional and post-transcriptional silencing. It was critical to know if TetR-GFP played a general role in this process. If so, it could be replaced by an analogous unrelated protein. Here we took advantage of the fact that each *tetO* site contains two GATA motifs (Fig. S1A), which can recruit GATA factors *in vivo* [41]. In *Neurospora*, upon nitrogen starvation, the GATA factor NIT-2 is known to activate the expression of genes involved in nitrogen catabolism [42]. The DNA binding domain of NIT-2 is very conserved (Fig. 3A), and its capacity to recognize

the GATA motif was demonstrated *in vitro* [42]. While only a few GATA motifs are found in the promoters of genes regulated by NIT-2 [43], the occurrence of many such motifs over the *tetO* array was expected to result in a situation where the aberrant activity of NIT-2 could perturb chromatin analogously to the strong binding of TetR-GFP.

To test the role of NIT-2, we created a new strain carrying only the *tetO* array, without the adjacent *lacO* array (Fig. 3B: 'Strain E'). This strain was also used to test for the *de novo* initiation of heterochromatin, as opposed to its spread from the *lacO* array. To this end, we found that, once TetR-GFP became available, the standalone *tetO* array expressed sRNAs and assembled H3K9me3 at the levels similar to those in Strain B (Fig. 3D,E: '+ *tetR-gfp*'), thus demonstrating the ability to initiate *de novo* transcriptional and post-transcriptional silencing.

Our basic nitrogen-starvation protocol included pre-growing *Neurospora* in the standard minimal medium for 24 hours, after which mycelial cultures were washed, transferred into a new medium lacking nitrogen, grown for additional 5 hours, and harvested for analyses (Fig. 3B,C). Thus, this protocol permitted assaying relevant parameters during the early stages of silencing. Remarkably, high levels of sRNAs and H3K9me3 were found at the *tetO* array upon nitrogen starvation, reaching those induced in the presence of the repressor (Fig. 3D,E). Critically, starvation-induced sRNAs and H3K9me3 were completely abrogated in the *nit-2Δ* condition (Fig. 3D,E,F). Genome-wide, several additional loci exhibited elevated levels of sRNAs upon starvation; for some of those loci this effect was dependent on NIT-2 (Fig. S8B).

Our further analysis revealed that the starvation-induced expression of *tetO*-derived sRNAs required QDE-1 and QDE-3 but not RAD51 or RAD52 (*tetO*-derived sRNAs decreased nearly 8-fold in the *rad52Δ* strain, yet they still exceeded background by two orders of magnitude; Fig. 3F). Thus, this process was classified as RIQ (Fig. 3F). Furthermore, starvation-induced assembly of constitutive heterochromatin occurred normally in the absence of QDE-1, QDE-3, RAD51 or RAD52 (Fig. S8A), excluding the roles of RNAi and recombination in its *de novo* initiation.

SAD-6 controls all starvation-induced silencing

Thus far, our results indicated that the silencing triggered by nitrogen starvation (and mediated by NIT-2) was equivalent to the silencing induced by TetR-GFP. Subsequent experiments established that the corresponding *sad-6Δ* conditions were also equivalent (Fig. 3D-J). Specifically, the following effects were noted at the array upon nitrogen starvation in the *sad-6Δ* strain: *tetO*-derived sRNAs were not induced (Fig. 3E,F), constitutive heterochromatin was not assembled (Fig. 3D), and the array became strongly nucleosome-depleted as well as MNase-hypersensitive (Fig. 3D,G-J). Interestingly, the array was essentially the only genomic locus featuring the aforementioned chromatin defects (Fig. S8C,D).

Comparison of high-resolution MNase-seq profiles yielded additional insights. First, MNase sensitivity of the unperturbed *tetO* array was not influenced by the adjacent heterochromatic *lacO* array (Fig. S7A,C: 'Strain A' and 'Strain E'). Second, when Strain E was starved for nitrogen, MNase sensitivity of the *tetO* array increased but remained largely uniform (Fig. S7A,C). Third, this uniformity was compromised in the *sad-6Δ* condition, recapitulating the state of the *tetO* array bound by TetR-GFP in the absence of SAD-6 (Fig. S7A,C). Notably, the two *sad-6Δ* conditions featured MNase-seq profiles that were markedly different, suggesting that the fine structure of the perturbed chromatin state was influenced by the nature of the perturbing agent.

DNA replication is required for starvation-induced RIQ

Canonical repeat-induced quelling can be suppressed by 0.1M hydroxyurea (HU) [44], a potent yet reversible inhibitor of DNA replication in *N. crassa* [45]. We also found that strong RIQ of the *tetO* array was dependent on the acetyltransferase RTT109 with known roles in DNA replication (Fig. 1C,F) [37]. Therefore, we asked if DNA replication was required for RIQ. Focusing first on the repressor-bound *tetO* array, we discovered that a 24-hour incubation of pre-grown mycelia in the minimal medium containing 0.1M HU downregulated *tetO*-derived sRNAs by a factor of 7 (while having no effect on *lacO*-derived sRNAs; Fig. 1C,F: 'Strain B + HU'). By microscopy, we confirmed that the repressor was still localized properly upon the HU treatment (Fig. S4). The enlarged size of the HU-treated nuclei and the increased proportion of background sRNAs were noticed (Fig. 1F; Fig. S4). This result indicated a possible connection between RIQ and DNA replication, yet because HU was added to the pre-grown mycelial cultures with already active RIQ, the magnitude of this effect could not be determined with certainty.

The above question was addressed using an experimental system provided by starvation-induced RIQ (Fig. 4). To block all DNA replication before starvation, HU was added during the last 5 hours of normal growth (Fig. 4A). Subsequently, the HU block could be either released or maintained during the starvation phase (Fig. 4A). Using this system, we found that maintaining the HU block suppressed all starvation-induced RIQ of the *tetO* array (Fig. 4B,C). The only other co-suppressed sRNAs were those expressed from AT-rich DNA (Fig. 4C).

The *lacO* array and native AT-rich DNA can undergo RIQ

Our results suggested that native AT-rich DNA and the *lacO* array shared the capacity to nucleate constitutive heterochromatin. In addition to constitutive heterochromatin, *Neurospora* features facultative heterochromatin marked by H3K27me3, which is deposited by the lysine methyltransferase SET-7 [23]. Compromised fitness of *dim-5Δ* strains can be partially restored by deleting *set-7+* [40,46]. Therefore, to analyze the expression of sRNAs from the *lacO* array and AT-rich DNA, we moved the *lacO–tetO* reporter to a new genetic background in which *dim-5+* and *set-7+* were both deleted (Fig. 5A: 'Strain C'). A matching *dim-5+* strain was created by

replacing *csr-1+* with the *dim-5+* transcription unit [16] (Fig. 5A: 'Strain D'). Our analysis of these otherwise isogenic strains suggested that DIM-5 promoted hH3 occupancy over AT-rich DNA and the *lacO* array, while also suppressing sRNA expression from these same regions (Fig. 5B,C; Fig. S9A). Affected sRNAs required QDE-1 but not RAD51, and they were also downregulated by HU (Fig. 5D; Fig. S9B-D). The roles of QDE-3 and RAD52 were not tested, because we were unable to delete *qde-3+* or *rad52+* in our basic *dim-5Δ* strain.

In the *dim-5Δ* condition, two results concerning the function of SAD-6 at AT-rich DNA were observed. First, SAD-6 was required for the optimal expression of most AT-rich sRNA loci suppressed by DIM-5 (Fig. 5D-F). Second, the loss of SAD-6 was associated with a broad increase in MNase sensitivity of AT-rich DNA (Fig. S9E,F). This effect was not evident for heterochromatinized AT-rich DNA (Fig. S6C). For the majority of the AT-rich loci engaged in RIQ, the increase in MNase sensitivity was moderate and largely uniform (Fig. S9F).

The *lacO* array becomes genetically unstable in the absence of heterochromatin

We found that the *lacO* array could still undergo RIQ in the absence of SAD-6 (Fig. S9D). This result was not surprising, as SAD-6 was also partially dispensable for RIQ of AT-rich DNA. However, in this *sad-6Δ* strain, approximately one half of the *lacO* array was deleted (Fig. S9D). Because such deletions were never observed in the other *sad-6Δ* strains, this result indicated that the *lacO* array became genetically unstable when stripped of heterochromatin. We used multiplex PCR to test the stability of the arrays in clonal populations of nuclei of several basic strains (Fig. S10). Two pairs of primers were mixed for each PCR. One pair was specific for the central portion of either the *lacO* or the *tetO* array, the second pair amplified a portion of *spo11* as the positive control (Fig. S10B). Using this approach, frequent deletions in the *lacO* array were uncovered, but only in the heterochromatin-deficient background (Fig. S10B: 'Strain C'). Such deletions corresponded to recombination products involving the three perfect repeats present in the *lacO* array (Fig. S1A). Thus, the *lacO* array differed from the *tetO* array in becoming genetically unstable in its perturbed state.

HDA1 and CHAP, members of the HCHC complex, play different roles at the *lacO* array

We next analyzed the role of constitutive heterochromatin in RIQ of the *lacO* array. In *N. crassa*, constitutive heterochromatin is controlled by several protein complexes, most notably by DCDC and HCHC [23]. DCDC catalyzes H3K9me3 and contains DIM-5 (the catalytic subunit), DIM-7, DIM-9, CUL4, and DDB1; whereas HCHC mediates histones deacetylation and contains HDA1 (the catalytic subunit), along with HP1, CDP-2, and CHAP [23]. With respect to DCDC, the loss of DIM-7 or DIM-9 affected the *lacO* array similarly to the loss of DIM-5: H3K9me3 was absent, the hH3 occupancy decreased, and RIQ became strongly activated (Fig. S9G-I). These results suggested that DIM-5, DIM-7, and DIM-9 played similar roles in maintaining the state of the *lacO* array, consistent with them being members of one protein complex.

A more nuanced outcome was observed regarding the function of the HCHC complex at the *lacO* array. While the loss of HDA1 largely recapitulated the loss of DCDC (Fig. S9G-I), the *lacO* array still featured high levels of hH3 and H3K9me3 without CHAP (Fig. S9G-I). Surprisingly, in this strain, the *lacO* array was also found to undergo RIQ (Fig. S9G-I). Genome-wide, the *hda1Δ* condition was associated with a moderate depletion of hH3 over AT-rich DNA; however, this effect was much less dramatic compared to that observed upon deleting *hda1+* in Strain B (Fig. S2C; Fig. S9I). These results suggested that, while HDA1 acted as a critical regulator of heterochromatin at the *lacO* array, CHAP was involved in fine-tuning the balance between heterochromatin formation and RIQ activation.

At the *lacO* array, RIQ can be decoupled from heterochromatin assembly

Our results showed that the *lacO* array could activate RIQ, assemble heterochromatin, and sustain high levels of genetic instability. It was interesting to know if any of those properties could be decoupled. To this end, we identified two clonal lineages of Strain C with spontaneous *lacO* deletions of 5247 and 8263 bps (Fig. S11A). The corresponding truncated arrays were named *d1* and *d2*, respectively (Fig. S11A). We found that *lacO(d1)* but not *lacO(d2)* could still induce RIQ (Fig. S11B). However, once DIM-5 was provided by transformation, both *lacO(d1)* and *lacO(d2)* became strongly heterochromatinized (Fig. S11C), suggesting that the ability of the *lacO* array to activate RIQ could be decoupled from its ability to assemble heterochromatin.

In principle, *lacO(d1)* could trigger RIQ because it contained some sequence motifs not present in *lacO(d2)*. Alternatively, a threshold amount of *lacO* DNA could be required. To differentiate between these possibilities, we generated three *dim-5Δ* strains with overlapping 1.4-1.6 kbp fragments of *lacO(d1)* (Fig. S11D,E). Neither fragment triggered RIQ; however, they all formed heterochromatin equally well once DIM-5 was provided by transformation (Fig. S11F,G). These results suggested that the ability to activate RIQ represented an emergent property of the *lacO* array, possibly controlled by a threshold-dependent mechanism.

DISCUSSION

The great diversity and abundance of repetitive DNA necessitated the evolution of various processes to keep this fraction of the genome in check. While some of these processes, including the KZFP-TRIM28-SETDB1 pathway in animals [1] and the RITS-CLRC relay in fission yeast [47], employ strong sequence-specific cues to target dispersed repeats, others become activated by a large number of repeats organized as tandem arrays [48]. Such processes were suggested to involve transcription-based mechanisms [48–50], homologous DNA-DNA pairing [16,51], and non-B-DNA structures [52,53]. Tandem repeats were also found to associate with diverse non-histone proteins, including transcription factors [48,54,55].

We have found that in *N. crassa*, transcriptional and post-transcriptional silencing can be induced *de novo* by the aberrant activities of two unrelated DNA binding proteins (a synthetic TetR repressor and the endogenous GATA factor NIT-2) at the *tetO* array. While transcriptional silencing was mediated by canonical constitutive heterochromatin, post-transcriptional silencing resembled quelling but still occurred in the absence of RAD51 or RAD52, two critical recombination factors. Therefore, this process was named recombination-independent quelling (RIQ). In both situations involving TetR-GFP or NIT-2, the *tetO* array featured perturbed chromatin, as evidenced by decreased nucleosome occupancy and high MNase sensitivity. This state was ameliorated by SAD-6, which was also needed to initiate all silencing at the *tetO* array. Moreover, the properties of perturbed chromatin associated with RIQ of the *tetO* array were also relevant for RIQ of native AT-rich DNA. Thus, the state of perturbed chromatin emerged as a general signal for silencing (Fig. 5G). Importantly, while the loss of nucleosomes was linked to all *de novo* silencing in this study, the exact nature of the inducing signal remains unknown. Other candidate signals include R-loops and non-canonical DNA structures, which are all expected to correlate with nucleosome occupancy.

At the *tetO* array, heterochromatin and RIQ are initiated concomitantly yet independently from one another. In principle, with respect to heterochromatin assembly, the role of SAD-6 may be similar to the role of ATRX in the deposition of histone H3.3, which also requires DAXX (although no fungal ortholog of DAXX has been identified) [11]. On the other hand, the role of SAD-6 in RIQ appears profoundly mysterious.

Recombination-independent quelling (RIQ) is a distinct RNAi process in *N. crassa*

Apart from quelling and MSUD, *N. crassa* sports two other RNAi pathways that can dynamically designate novel sRNA-producing loci [56]. The first (qiRNA) pathway is linked to DNA damage and requires RAD51 and RAD52, as well as the classical quelling factors QDE-1 and QDE-3 [56]. The second (disiRNA) pathway targets non-repetitive loci associated with sense/antisense transcription, does not require QDE-1 and QDE-3 [35], but depends on the exonuclease ERI1 [34]. Our results set these processes apart from RIQ (which needs QDE-1 and QDE-3 but not RAD51, RAD52, or ERI1). Yet RIQ and canonical quelling share the requirement for DNA replication and the H3K56 acetyltransferase RTT109 (which is also linked to DNA replication) [37]. In the case of RIQ, replication may be required to generate nascent chromatin [57], which may be particularly prone to perturbation by the aberrant activity of some DNA binding proteins (such as TetR-GFP and NIT-2).

Several types of RIQ appear to exist with respect to the requirement for SAD-6. While RIQ of the *tetO* array induced by TetR-GFP is absolutely dependent on SAD-6, low levels of *tetO*-derived sRNAs are still observed without SAD-6 upon nitrogen starvation. Further, RIQ of AT-rich DNA is only partially dependent on SAD-6, and RIQ of the *lacO* array occurs normally without SAD-6, implying that SAD-6 can be replaced by another factor (altogether, the *N. crassa* genome encodes 24 ATPases with predicted chromatin-remodeling functions

[58]). Nevertheless, all types of RIQ involve perturbed chromatin, require QDE-1, and occur without RAD51, the only RecA-like recombinase in *N. crassa* [58]. All types of RIQ must also rely on transcription to produce single-stranded RNA that can be used as a template for synthesizing double-stranded RNA. While QDE-1 was proposed to mediate this step in the qiRNA pathway [59], the nature of the DNA-dependent RNA polymerase at the basis of RIQ remains unknown.

In *Neurospora*, two peculiar populations of sRNAs were previously described: one population corresponds to subtelomeric sRNAs, the other comprises sRNAs expressed at low background levels throughout the genome [35]. Notably, we have found that the levels of background sRNAs were apparently increased in all conditions linked to replication and recombination defects. In a subset of these conditions (specifically, without RAD51, RAD52, or RTT109), the levels of subtelomeric sRNAs became elevated as well. Neither of these effects was associated with the loss of QDE-3, consistent with the idea that QDE-3 plays a redundant role in DNA repair [60].

Role of chromatin remodeling in the *de novo* initiation of silencing

The role of ATP-dependent remodelers in heterochromatin (re)assembly has been well established, with some archetypal examples including (in addition to ATRX-DAXX) the nucleolar remodeling complex (NoRC) [61], the nucleosome remodeling and deacetylase (NuRD) complex [62], Snf2/Hdac-containing repressor complex (SHREC) [63], as well as the helicases SMARCAD1 [64], HELLS/LSH [65] and its plant counterpart DDM1 [66,67]. These factors make nucleosomes more accessible or replaced altogether to promote the incorporation of histone variants or modifications favoring heterochromatin. Our results suggest that the aberrant activity of DNA binding proteins can produce a state of perturbed chromatin that may constitute a particularly favorable substrate for the remodeling-dependent silencing. Curiously, the occurrence of diverse transcription factors at mammalian pericentromeres was reported [48,54,55]. While some of these factors could induce the silencing directly, by recruiting additional enzymatic activities or driving transcription of non-coding RNAs [54], others may do so indirectly, by producing a state of perturbed chromatin. In budding yeast, the tight binding of LacI and TetR repressors to their operator arrays was shown to trigger transcriptional silencing [30,31]. According to our data, this process (i) can be induced by other DNA binding proteins, (ii) requires chromatin remodeling, and (iii) may also initiate post-transcriptional silencing.

How does SAD-6 recognize perturbed chromatin? Because SAD-6 controls RIQ of diverse loci (*i.e.*, the *tetO* array versus AT-rich DNA), it is unlikely to rely on sequence-specific signals or secondary structures that may recruit its orthologs in other situations [68]. On the other hand, SAD-6-dependent RIQ is associated with low nucleosome occupancy and high MNase sensitivity, suggesting that SAD-6 may favor nucleosome-free DNA. This propensity is shared by metazoan ATRX, which also localizes to nucleosome-depleted regions, including

heavily transcribed genes [12], free proviral DNA [69], and R-loops [13]. In human cells, 87% of ATRX sites are present in open chromatin [70], and ATRX was also shown to interact with free nucleic acids *in vitro* [71]. Yet the exact nature of the SAD-6 recruitment mechanism and its relationship with the initiation of silencing all remain to be established.

In this study, the state of perturbed chromatin was induced by the aberrant activities of non-histone proteins at the *tetO* array. Yet, an analogous state might also be attained by other means, for example, by recombination-independent homologous pairing [72]. This idea is supported by the role of SAD-6 in MSUD, which relies on such pairing to find gaps in sequence identity between homologous chromosomes [20,22]. Thus, the proposed model (Fig. 5G), although derived from a synthetic experimental system, may also underpin other instances of the *de novo* initiation of transcriptional and post-transcriptional silencing in eukaryotes.

ACKNOWLEDGMENTS

The work was supported by Agence Nationale de la Recherche (ANR-10-LABX-0062, ANR-11-LABX-0044, ANR-10-IDEX-0001-02, ANR-19-CE12-0002) and Institut Pasteur. We also acknowledge the Cell and Tissue Imaging Platform “PICT-IBiSA” (the Pasteur Imaging Facility, Institut Curie, part of the France Bioimaging National Infrastructure, funded by ANR-10-INBS-04).

AUTHOR CONTRIBUTIONS

F.C. and E.G. designed research; F.C., S.C.R., J.K., S.C., I.L., and E.G. performed research; E.G. contributed new analytic tools; F.C., I.L., A.T., and E.G. analyzed data; E.G. wrote the paper.

DECLARATION OF INTERESTS

The authors declare no competing interests.

DATA, MATERIALS, AND SOFTWARE AVAILABILITY

All NGS data produced in this study were submitted to the Short Read Archive (BioProject PRJNA1109611). All strains created and analyzed in this study were submitted to the Fungal Genetics Stock Center (accessions 27332-27373). Custom genome references created and used in this study are available at figshare.com (DOI: 10.6084/m9.figshare.24943173.

MATERIALS AND METHODS SUMMARY

A combination of ChIP-seq, MNase-seq, and sRNA-seq approaches was used to analyze the state of synthetic repetitive loci (represented by the *lacO* and the *tetO* operator arrays) and native AT-rich DNA. The following

processes were assayed: (i) formation of constitutive heterochromatin, (ii) histone occupancy, (3) sensitivity to MNase, and (4) sRNAs expression.

REFERENCES

1. Almeida, M.V. *et al.* (2022) Taming transposable elements in vertebrates: from epigenetic silencing to domestication. *Trends Genet* 38, 529–553
2. Allshire, R.C. and Madhani, H.D. (2018) Ten principles of heterochromatin formation and function. *Nat Rev Mol Cell Biol* 19, 229–244
3. Janssen, A. *et al.* (2018) Heterochromatin: Guardian of the Genome. *Annu. Rev. Cell Dev. Biol.* 34, 265–288
4. Hamel, J. and Tawil, R. (2018) Facioscapulohumeral Muscular Dystrophy: Update on Pathogenesis and Future Treatments. *Neurotherapeutics* 15, 863–871
5. Bull, J.H. and Wootton, J.C. (1984) Heavily methylated amplified DNA in transformants of *Neurospora crassa*. *Nature* 310, 701–704
6. Ye, F. and Signer, E.R. (1996) RIGS (repeat-induced gene silencing) in Arabidopsis is transcriptional and alters chromatin configuration. *Proc Natl Acad Sci U S A* 93, 10881–10886
7. Dorer, D.R. and Henikoff, S. (1994) Expansions of transgene repeats cause heterochromatin formation and gene silencing in Drosophila. *Cell* 77, 993–1002
8. Garrick, D. *et al.* (1998) Repeat-induced gene silencing in mammals. *Nature Genetics* 18, 56–59
9. Blewitt, M.E. *et al.* (2005) An N-ethyl-N-nitrosourea screen for genes involved in variegation in the mouse. *Proc Natl Acad Sci U S A* 102, 7629–7634
10. Daxinger, L. *et al.* (2013) An ENU mutagenesis screen identifies novel and known genes involved in epigenetic processes in the mouse. *Genome Biol* 14, R96
11. Aguilera, P. and López-Contreras, A.J. (2023) ATRX, a guardian of chromatin. *Trends in Genetics* 39, 505–519
12. Schneiderman, J.I. *et al.* (2012) Nucleosome-depleted chromatin gaps recruit assembly factors for the H3.3 histone variant. *Proc Natl Acad Sci U S A* 109, 19721–19726
13. Nguyen, D.T. *et al.* (2017) The chromatin remodelling factor ATRX suppresses R-loops in transcribed telomeric repeats. *EMBO Rep* 18, 914–928
14. Selker, E.U. (1990) Premeiotic instability of repeated sequences in *Neurospora crassa*. *Annu. Rev. Genet.* 24, 579–613
15. Gladyshev, E. (2017) Repeat-Induced Point Mutation and Other Genome Defense Mechanisms in Fungi. *Microbiol Spectr* 5, 5.4.02
16. Gladyshev, E. and Kleckner, N. (2017) DNA sequence homology induces cytosine-to-thymine mutation by a heterochromatin-related pathway in Neurospora. *Nat Genet* 49, 887–894

17. Romano, N. and Macino, G. (1992) Quelling: transient inactivation of gene expression in *Neurospora crassa* by transformation with homologous sequences. *Mol Microbiol* 6, 3343–3353
18. Shiu, P.K.T. *et al.* (2001) Meiotic silencing by unpaired DNA. *Cell* 107, 905–916
19. Hammond, T.M. (2017) Sixteen years of meiotic silencing by unpaired DNA. *Ndv. Genet.* 97, 1–42
20. Rhoades, N. *et al.* (2021) Recombination-independent recognition of DNA homology for meiotic silencing in *Neurospora crassa*. *Proc Natl Acad Sci U S A* 118, e2108664118
21. Zhang, Z. *et al.* (2013) Homologous recombination as a mechanism to recognize repetitive DNA sequences in an RNAi pathway. *Genes Dev* 27, 145–150
22. Samarajeewa, D.A. *et al.* (2014) Efficient detection of unpaired DNA requires a member of the rad54-like family of homologous recombination proteins. *Genetics* 198, 895–904
23. Aramayo, R. and Selker, E.U. (2013) *Neurospora crassa*, a model system for epigenetics research. *Cold Spring Harb Perspect Biol* 5, a017921
24. Smith, K.M. *et al.* (2010) H2B- and H3-specific histone deacetylases are required for DNA methylation in *Neurospora crassa*. *Genetics* 186, 1207–1216
25. Klocko, A.D. *et al.* (2019) Nucleosome Positioning by an Evolutionarily Conserved Chromatin Remodeler Prevents Aberrant DNA Methylation in Neurospora. *Genetics* 211, 563–578
26. Belden, W.J. *et al.* (2011) CHD1 remodels chromatin and influences transient DNA methylation at the clock gene frequency. *PLoS Genet* 7, e1002166
27. Dang, Y. *et al.* (2013) Convergent transcription induces dynamic DNA methylation at disiRNA loci. *PLoS Genet* 9, e1003761
28. Ruesch, C.E. *et al.* (2014) The histone H3 lysine 9 methyltransferase DIM-5 modifies chromatin at frequency and represses light-activated gene expression. *G3 (Bethesda)* 5, 93–101
29. Nguyen, T.-S. and Gladyshev, E. (2020) Developing a tetO/TetR system in *Neurospora crassa*. *Fungal Genet Biol* 136, 103316
30. Loïodice, I. *et al.* (2021) An Inducible System for Silencing Establishment Reveals a Stepwise Mechanism in Which Anchoring at the Nuclear Periphery Precedes Heterochromatin Formation. *Cells* 10, 2810
31. Dubarry, M. *et al.* (2011) Tight protein-DNA interactions favor gene silencing. *Genes Dev* 25, 1365–1370
32. Lau, I.F. *et al.* (2003) Spatial and temporal organization of replicating Escherichia coli chromosomes. *Mol Microbiol* 49, 731–743
33. Forrest, E.C. *et al.* (2004) The RNA-dependent RNA polymerase, QDE-1, is a rate-limiting factor in post-transcriptional gene silencing in *Neurospora crassa*. *Nucleic Acids Res* 32, 2123–2128
34. Dang, Y. *et al.* (2016) Antisense transcription licenses nascent transcripts to mediate transcriptional gene silencing. *Genes Dev* 30, 2417–2432

35. Lee, H.-C. *et al.* (2010) Diverse pathways generate microRNA-like RNAs and Dicer-independent small interfering RNAs in fungi. *Mol Cell* 38, 803–814
36. Zhang, Z. *et al.* (2014) Histone H3K56 acetylation is required for quelling-induced small RNA production through its role in homologous recombination. *J Biol Chem* 289, 9365–9371
37. Dahlin, J.L. *et al.* (2015) Histone-modifying enzymes, histone modifications and histone chaperones in nucleosome assembly: Lessons learned from Rtt109 histone acetyltransferases. *Crit Rev Biochem Mol Biol* 50, 31–53
38. Symington, L.S. *et al.* (2014) Mechanisms and regulation of mitotic recombination in Saccharomyces cerevisiae. *Genetics* 198, 795–835
39. Lu, M. and He, X. (2019) Intricate regulation on epigenetic stability of the subtelomeric heterochromatin and the centromeric chromatin in fission yeast. *Curr Genet* 65, 381–386
40. Basenko, E.Y. *et al.* (2015) Genome-wide redistribution of H3K27me3 is linked to genotoxic stress and defective growth. *Proc Natl Acad Sci U S A* 112, E6339-6348
41. Gould, D.J. and Chernajovsky, Y. (2004) Endogenous GATA factors bind the core sequence of the tetO and influence gene regulation with the tetracycline system. *Mol Ther* 10, 127–138
42. Fu, Y.H. and Marzluf, G.A. (1990) nit-2, the major positive-acting nitrogen regulatory gene of *Neurospora crassa*, encodes a sequence-specific DNA-binding protein. *Proc Natl Acad Sci U S A* 87, 5331–5335
43. Huberman, L.B. *et al.* (2021) DNA affinity purification sequencing and transcriptional profiling reveal new aspects of nitrogen regulation in a filamentous fungus. *Proc Natl Acad Sci U S A* 118, e2009501118
44. Nolan, T. *et al.* (2008) The RNA-dependent RNA polymerase essential for post-transcriptional gene silencing in *Neurospora crassa* interacts with replication protein A. *Nucleic Acids Res* 36, 532–538
45. Sachs, M.S. *et al.* (1997) Expression of herpes virus thymidine kinase in *Neurospora crassa*. *Nucleic Acids Res* 25, 2389–2395
46. Jamieson, K. *et al.* (2016) Loss of HP1 causes depletion of H3K27me3 from facultative heterochromatin and gain of H3K27me2 at constitutive heterochromatin. *Genome Res* 26, 97–107
47. Holoch, D. and Moazed, D. (2015) RNA-mediated epigenetic regulation of gene expression. *Nat Rev Genet* 16, 71–84
48. Saksouk, N. *et al.* (2015) Constitutive heterochromatin formation and transcription in mammals. *Epigenetics & Chromatin* 8, 1600–1614
49. Zhou, J. *et al.* (2023) DDM1-mediated R-loop resolution and H2A.Z exclusion facilitates heterochromatin formation in Arabidopsis. *Sci Adv* 9, eadg2699
50. Skourti-Stathaki, K. *et al.* (2014) R-loops induce repressive chromatin marks over mammalian gene terminators. *Nature* 516, 436–439

51. Carlier, F. *et al.* (2021) Modulation of C-to-T mutation by recombination-independent pairing of closely positioned DNA repeats. *Biophysical Journal* 120, 4325–4336
52. Herbert, A. (2020) ALU non-B-DNA conformations, flipons, binary codes and evolution. *R. Soc. open sci.* 7, 200222
53. Wang, G. and Vasquez, K.M. (2023) Dynamic alternative DNA structures in biology and disease. *Nat Rev Genet* 24, 211–234
54. Saksouk, N. *et al.* (2014) Redundant mechanisms to form silent chromatin at pericentromeric regions rely on BEND3 and DNA methylation. *Mol Cell* 56, 580–594
55. Bulut-Karslioglu, A. *et al.* (2012) A transcription factor-based mechanism for mouse heterochromatin formation. *Nat Struct Mol Biol* 19, 1023–1030
56. Dang, Y. *et al.* (2014) Small RNA-Mediated Gene Silencing in Neurospora. In *Fungal RNA Biology* (Sesma, A. and Von Der Haar, T., eds), pp. 269–289, Springer International Publishing
57. MacAlpine, D.M. and Almouzni, G. (2013) Chromatin and DNA replication. *Cold Spring Harb Perspect Biol* 5, a010207
58. Borkovich, K.A. *et al.* (2004) Lessons from the genome sequence of *Neurospora crassa*: tracing the path from genomic blueprint to multicellular organism. *Microbiol Mol Biol Rev* 68, 1–108
59. Lee, H.-C. *et al.* (2009) qiRNA is a new type of small interfering RNA induced by DNA damage. *Nature* 459, 274–277
60. Kato, A. and Inoue, H. (2006) Growth defect and mutator phenotypes of RecQ-deficient *Neurospora crassa* mutants separately result from homologous recombination and nonhomologous end joining during repair of DNA double-strand breaks. *Genetics* 172, 113–125
61. Postepska-Igielska, A. *et al.* (2013) The chromatin remodelling complex NoRC safeguards genome stability by heterochromatin formation at telomeres and centromeres. *EMBO Rep* 14, 704–710
62. Helbling Chadwick, L. *et al.* (2009) The Mi-2/NuRD complex associates with pericentromeric heterochromatin during S phase in rapidly proliferating lymphoid cells. *Chromosoma* 118, 445–457
63. Sugiyama, T. *et al.* (2007) SHREC, an Effector Complex for Heterochromatic Transcriptional Silencing. *Cell* 128, 491–504
64. Rowbotham, S.P. *et al.* (2011) Maintenance of silent chromatin through replication requires SWI/SNF-like chromatin remodeler SMARCAD1. *Mol Cell* 42, 285–296
65. Yu, W. *et al.* (2014) Genome-wide DNA methylation patterns in LSH mutant reveals de-repression of repeat elements and redundant epigenetic silencing pathways. *Genome Res* 24, 1613–1623
66. Osakabe, A. *et al.* (2021) The chromatin remodeler DDM1 prevents transposon mobility through deposition of histone variant H2A.W. *Nat Cell Biol* 23, 391–400
67. Lee, S.C. *et al.* (2023) Chromatin remodeling of histone H3 variants by DDM1 underlies epigenetic inheritance of DNA methylation. *Cell* 186, 4100-4116.e15

68. Teng, Y.-C. *et al.* (2021) ATRX promotes heterochromatin formation to protect cells from G-quadruplex DNA-mediated stress. *Nat Commun* 12, 3887
69. Lukashchuk, V. *et al.* (2008) Human cytomegalovirus protein pp71 displaces the chromatin-associated factor ATRX from nuclear domain 10 at early stages of infection. *J Virol* 82, 12543–12554
70. Truch, J. *et al.* (2022) The chromatin remodeller ATRX facilitates diverse nuclear processes, in a stochastic manner, in both heterochromatin and euchromatin. *Nat Commun* 13, 3485
71. Sarma, K. *et al.* (2014) ATRX directs binding of PRC2 to Xist RNA and Polycomb targets. *Cell* 159, 869–883
72. Mazur, A.K. and Gladyshev, E. (2023) C-DNA may facilitate homologous DNA pairing. *Trends Genet* 39, 575–585

FIGURE LEGENDS

Figure 1. Repressor-bound *tetO* array initiates transcriptional and post-transcriptional silencing.

(A) Series of strains created by homologous transformations, as indicated (strain identifications and complete genotypes are provided in Table S2).

(B) Properties of sRNAs expressed from the repressor-bound *tetO* array (in Strain B).

(C) Changes in the expression of array-derived sRNAs (see text for explanation). Corresponding raw data are plotted in Fig. 1F.

(D) Density of ChIP-seq reads over the *lacO–tetO* reporter and the neighboring genes (per 1 bp, per 1 million mapped reads). Unless noted otherwise, all profiles are plotted to the same scale, corresponding to the default scale bar in the upper right corner. Tc: cultures were supplemented with tetracycline (100 μg/μl). The plotted region is 26000-bp long.

(E) Density of sRNA-seq reads over the *lacO–tetO* reporter and the neighboring genes (analyzed and plotted as in Fig. 1D).

(F) Scatter plots showing genome-wide changes in sRNA expression. The number of reads (expressed per 500 bp, per 1 million mapped reads) was augmented by 1 to enable log transformation. Tiles overlapping the *lacO* array, the *tetO* array, and the reference loci correspond to pink, green, and light-blue circles, respectively. Populations of sRNAs expressed from subtelomeric and AT-rich regions are marked by magenta and blue arrows, respectively.

Figure 2. Chromatin remodeler SAD-6 controls all silencing of the repressor-bound *tetO* array.

(A) Scatter plot showing genome-wide changes in sRNA expression (analyzed and plotted as in Fig. 1F).

(B) Density of ChIP-seq reads over the arrays and the neighboring genes (analyzed and plotted as in Fig. 1D).

(C) Scatter plots showing the relationship between MNase sensitivity and GC-content (plotted in Fig. S1E). Tiles overlapping the *lacO* and the *tetO* arrays are shown as pink and green circles, respectively.
(D) Density of ChIP-seq reads over the arrays and the neighboring genes (analyzed and plotted as in Fig. 1D).
(E) Scatter plots showing the relationship between histone occupancy and GC-content. Strongly nucleosome-depleted (SND) tiles were defined as those having the log10-transformed (IP[hH3]+1)/(Input+1) ratio of -0.5 or less. Tiles overlapping the *lacO* and the *tetO* arrays are shown as pink and green circles, respectively.
(F) Histogram showing the relationship between the length and the number of strongly nucleosome-depleted (SND) regions. The length of SND regions corresponds to the number of consecutive SND tiles included in this region.
(G) Density of ChIP-seq reads over the arrays and the neighboring genes (analyzed and plotted as in Fig. 1D).

Figure 3. Nitrogen starvation induces silencing of the *tetO* array in the absence of the repressor.
(A) Comparison of the DNA binding domains of NIT-2 and its yeast ortholog Gat1.
(B) Series of strains created by homologous transformations, as indicated (strain identifications and complete genotypes are provided in Table S2).
(C) Standard protocol for inducing acute nitrogen starvation.
(D) Density of ChIP-seq reads over the array and the neighboring genes (analyzed and plotted as in Fig. 1D).
(E) Density of sRNA-seq reads over the array and the neighboring genes (analyzed and plotted as in Fig. 1E).
(F) Scatter plots showing genome-wide changes in sRNA expression (analyzed and plotted as in Fig. 1F). Tiles overlapping the *tetO* array and the reference loci are shown as green and light-blue circles, respectively.
(G) Density of ChIP-seq reads over the array and the neighboring genes (analyzed and plotted as in Fig. 1D).
(H) Scatter plots showing the relationship between histone occupancy and GC-content (nitrogen starvation in the absence of SAD-6; analyzed and plotted as in Fig. 2E).
(I) Histogram showing the relationship between the length and the number of strongly nucleosome-depleted (SND) regions (analyzed and plotted as in Fig. 2F).
(J) Scatter plots showing the relationship between MNase sensitivity and GC-content (analyzed and plotted as in Fig. 2C).

Figure 4. DNA replication is required for post-transcriptional silencing induced by nitrogen starvation.
(A) Modifications of the standard nitrogen-starvation protocol (Fig. 3C), which include treatments with 0.1M hydroxyurea (HU) before and (optionally) during starvation.
(B) Density of sRNA-seq reads over the array and the neighboring genes (analyzed and plotted as in Fig. 1E).
(C) Scatter plot showing the relationship between changes in sRNA expression and GC-content.

Figure 5. SAD-6 also regulates post-transcriptional silencing of native AT-rich DNA.

(A) Series of strains created by homologous transformations, starting from Strain C (strain identifications and complete genotypes are provided in Table S2). Strain C was produced by crossing Strain A with another strain carrying *dim-5Δ* and *set-7Δ* (Table S2).

(B) Scatter plot showing the relationship between changes in sRNA expression and GC-content (analyzed and plotted as in Fig. 4C). Tiles overlapping the *lacO* and the *tetO* arrays are shown as pink and green circles, respectively.

(C) Scatter plots showing the relationship between histone occupancy and GC-content (analyzed and plotted as in Fig. 2E).

(D) Scatter plots showing genome-wide changes in sRNA expression (analyzed as in Fig. 1F). Populations of sRNAs affected differentially by the deletions of *qde-1+* and *sad-6+* in Strain C are indicated (brown arrows). Reference loci are shown as light-blue circles.

(E) Changes in sRNA expression across Chromosome I, obtained as ratios of sRNA-seq reads using the same array of 500-bp tiles as in Fig. 1F. All denominator values were augmented by 1.

(F) Euler diagrams showing the relationships among several groups of genomic loci (represented by the same set of 500-bp tiles as in Fig. 1F). AT-rich DNA is defined by GC-content ≤ 38%. Other thresholds correspond to the five-fold change in sRNA expression.

(G) Chromatin can exist in two states, normal and perturbed. Perturbed state can be promoted by the aberrant activities of DNA-binding proteins, such as TetR-GFP or NIT-2. Chromatin can be returned to its normal state by dedicated chromatin remodelers, such as SAD-6, which are also required to initiate the *de novo* silencing.

SUPPORTING INFORMATION (SI)

MATERIALS AND METHODS

Plasmids

Plasmids were made by standard molecular cloning and validated by Sanger sequencing. Plasmid pFOC104A (carrying *lacO–tetO*) was made by inserting the NheI–XbaI fragment of pLAU43 [32] into pTSN6 [29]. This plasmid was propagated in *E. coli* DH10B cells in the presence of gentamicin and kanamycin [32]. All gene-deletion plasmids contained a marker conferring resistance to nourseothricin (clonNAT). Maps of all plasmids used in this study are provided in SI Data File 1.

Manipulation of *Neurospora* strains

A. Strains

All *Neurospora* strains used in this study are listed in Table S2. All genes analyzed in this study are described in Table S1.

B. Growth Media

Vogel's minimal medium N with 1.5% sucrose ('VM medium') was used for standard vegetative growth. The same medium but lacking ammonium nitrate ('VM-N medium) was used to induce acute nitrogen starvation. If needed, these media were supplemented with 100 µg/µl tetracycline, 0.1 µg/µl blasticidin S (to increase the expression of FLAG-SAD-6), or 0.1M hydroxyurea. Colonial growth was produced on sorbose agar (1x VM salts, 3% agar, 2% sorbose, 0.1% dextrose). For crossing, Synthetic Cross medium was used [73], containing 2% sucrose, 0.2 µg/ml biotin, and 2% agar. Crosses were setup on agar slants in glass culture tubes (20 x 200 mm). Ejected ascospores were collected in drops of water, induced by heat (60 ºC for 30 min), and plated on sorbose agar at appropriate dilutions.

C. Transformations

20 µl of macroconidia (washed and pelleted in 1M sorbitol) were combined with 1-2 µg of linearized plasmid DNA (dissolved in 10 µl of 1M sorbitol), incubated on ice for 20 min, and electroporated using the following settings: 1500 V, 600 Ω, 25 µF, 2 mm gap. Immediately following electroporation, macroconidia were mixed with 1 ml of 1M sorbitol. When transformed with plasmids targeting *his-3* or *csr-1*, macroconidia were plated on sorbose agar without delay. When transformed with plasmids carrying the nourseothricin resistance gene, macroconidia were allowed to recover for 4-5 hours at room temperature prior to being plated on sorbose agar supplemented with 50 µg/ml nourseothricin (Jena Bioscience, cat. no. AB-101L). Colonies were picked using glass Pasteur pipettes. Genomic DNA was prepared as previously described [74], and integration events were analyzed by PCR. Homokaryotic strains were obtained from primary transformants by macroconidiation. The

integrity of the *lacO–tetO* locus was verified using the Expand Long Template PCR System (Roche) with the following primer pairs: P1/P3, P2/P5, P4/P7, and P6/P8 (Table S3). The *tetO* locus was verified analogously, using the primer pairs P1/P7 and P6/P8 (Table S3).

Assaying genetic stability of the arrays by multiplex PCR

Genomic DNA was extracted as previously described [74]. Two separate master mixes were prepared. Both mixes contained primers P9 and P10 (Table S3), which amplified a portion of the *spo11+* gene (as a positive control). In addition, the first master mix included primers P2 and P3 (to amplify the central part of the *lacO* array), while the second master mix included primers P6 and P7 (to amplify the central part of the *tetO* array). PCR products were resolved on 1.5% agarose gels and imaged using Gel Doc EZ (Bio-Rad).

Standard nitrogen starvation protocol

Each culture was started by inoculating thawed macroconidia (~1 million CFUs) into 150 ml of VM medium. Cultures were grown for 24 hours at 30 ºC/180 RPM. Resultant mycelia were transferred into chilled vacuum filtration units and rinsed 5 times with 100 ml of chilled water. Each mycelial sample was placed into 150 ml of VM-N medium and incubated for 5 hours at 30 ºC/180 RPM. Mycelia were collected by filtration and split into two halves. One half was crosslinked using formaldehyde (described below), the other half was squeeze-dried and frozen in liquid nitrogen immediately.

Nitrogen starvation protocol including treatment with hydroxyurea (HU)

Each culture was started by inoculating thawed macroconidia (~1 million CFUs) into 130 ml of VM medium. Cultures were pre-grown for 19 hours at 30 ºC/180 RPM, adjusted to 130 g, supplemented with 20 ml of VM medium containing 1.14 g of HU, and returned to growth for additional 5 hours at 30 ºC/180 RPM. Resultant mycelia were transferred into chilled vacuum filtration units, rinsed 5 times with 100 ml of chilled water, and returned to growth (5 hours, 30 ºC/180 RPM) either in 150 ml of pure VM-N medium or in 150 ml of VM-N medium supplemented with 0.1M HU. Mycelia were collected by filtration and split into two halves. One half was crosslinked using formaldehyde (described below), the other half was squeeze-dried and frozen in liquid nitrogen immediately.

Chromatin immunoprecipitation (ChIP)

Each culture was started by inoculating thawed macroconidia (~1 million CFUs) into 150 ml of VM medium. Cultures were grown for 24 hours at 30 ºC/180 RPM. Resultant mycelia were collected by filtration, washed with phosphate-buffered saline (PBS) at room temperature, squeeze-dried, and transferred into 100 ml of PBS containing 1% formaldehyde. Crosslinking proceeded for 30 min at room temperature with constant stirring. After quenching with glycine for 5 min, mycelia were collected by filtration, rinsed with PBS, squeeze-dried,

ground to fine powder in liquid nitrogen, and stored at -80 ºC. The same mycelial prep was used for ChIP-seq and MNase-seq experiments.

For each sample, 150 mg of mycelial powder were combined with 1 ml of lysis buffer [140 mM NaCl; 1 mM EDTA; 1% Triton X-100; 0.1% sodium deoxycholate; 50 mM HEPES pH 7.5] containing 20 µl of proteinase inhibitors (Roche, cat. no. 11873580001, one tablet dissolved in 1 ml of PBS). Samples were transferred into 15-ml TPX tubes and sonicated in Bioruptor Plus (Diagenode) with the following settings: high power mode, 20 cycles, 90/90 sec ON/OFF, 4 ºC. After sonication, samples were centrifuged twice for 5 min at 13000 ×g, 4 ºC. SureBeads Protein A Magnetic Beads (Bio-Rad) were used for immunoprecipitation. Concentrated beads were washed and diluted five-fold in lysis buffer. The workflow included the following steps. First, each ChIP sample was pre-cleared using 20 µl of diluted beads (4 hours at 4 ºC). Second, 25 µl of each pre-cleared ChIP sample were saved as 'Input'. Third, an appropriate antibody (0.5-1.0 µl) was added and allowed to recognize its targets overnight (at 4 ºC). The following antibodies were used: anti-FLAG (Sigma F1804), anti-H3K9me3 (Active Motif AB_2532132), anti-hH2B (Abcam ab1790), anti-hH3 (Abcam ab1791), and anti-GFP (Abcam ab290). Fourth, 20 µl of diluted beads, washed in lysis buffer containing 0.1% Tween-20, were added to each sample and incubated for 4 hours at 4 ºC (all incubations were done using a rotating wheel). Fifth, beads were washed in the following buffers (1 ml, for 10 min): [i] lysis buffer (twice), [ii] lysis buffer with 0.5M NaCl, [iii] wash buffer [250 mM LiCl; 0.5% IGEPAL; 0.5% sodium deoxycholate; 1 mM EDTA; 10 mM TrisHCl pH 8.0], and {iv} TE buffer [1 mM EDTA; 10 mM TrisHCl pH 8.0]. Elution was done using TES buffer [1% SDS; 10 mM EDTA; 50 mM TrisHCl pH 8.0], for 10 min at 65 °C. Input fractions were also treated with TES buffer in parallel. Fractions were decrosslinked at 65 °C overnight, treated with RNAse A and then Proteinase K. DNA was purified by phenol-chloroform extraction, precipitated with ethanol, resuspended in 20 µl of TE buffer, and quantified using the Qubit dsDNA HS assay kit (Invitrogen). Two separate cultures (representing independent biological replicates) were analyzed for each condition.

MNase sensitivity analysis

For each sample, 80 mg of crosslinked mycelial powder were combined with 1 ml of lysis buffer including 20 µl of proteinase inhibitors (prepared as described above) and 2 mM $CaCl_2$. Samples were mixed, equilibrated on ice for 10 min, mixed again, supplemented with 10 µl of MNase (NEB, cat. no. M0247S), and incubated in ThermoMixer C (Eppendorf) for 30 min at 37 ºC. Reactions were stopped by adding 30 µl of 0.5M EGTA pH 8.0. Samples were centrifuged twice for 10 min at 16000 ×g, 4 ºC. For decrosslinking, 50 µl of each sample were combined with 200 µl of TES buffer and incubated at 65 °C overnight, after which samples were treated with RNAse A and then Proteinase K. DNA was purified analogously to the ChIP protocol, and resuspended in 30 µl of TE buffer. DNA concentrations were measured using the Qubit dsDNA HS assay kit (Invitrogen).

Preparing ChIP-seq and MNase-seq libraries

ChIP-seq and MNase-seq libraries were made using the NEBNext Ultra II DNA Library Prep Kit for Illumina (NEB, cat. no. E7645S) and Agencourt Ampure XP beads (Beckman Coulter, cat. no. A63880), following the manufacturer's instructions. Depending on the amount of starting material, libraries were amplified with 10-11 cycles of PCR. All ChIP-seq and MNase-seq libraries created and analyzed in this study are listed in Table S4 and Table S5, respectively.

Isolating small RNAs

Total RNA was extracted from ground mycelia with TRI Reagent (Sigma-Aldrich) and dissolved in 5M urea. RNA with a RINe score above 9.5 (as determined by the 4150 TapeStation System) was fractionated on 8% TBE-Urea gels. Approximately 60 µg of RNA were loaded on each gel, distributed in 6 wells. Populations of small RNAs in the 17-26 nt range were excised as gel slices. The latter were crushed and incubated overnight in 0.3 M NaCl at 25 ºC/850 RPM. Gel debris was removed using 0.22-µm spin columns (Sigma-Aldrich, cat. no. CLS8161). Small RNAs were precipitated by adding 4 volumes of ethanol and centrifuging for 40 min at 20000 ×g, 4 ºC. Pellets were dissolved in the total volume of 12 µl of water (per gel). Two separate cultures (representing independent biological replicates) were analyzed for each condition.

Preparing sRNA-seq libraries

sRNA-seq libraries were made as previously described [20]. For each library, 5 µl of sRNA sample were used, corresponding to 25 µg of input RNA (however, because a fraction of sRNAs was lost during purification, the amount of total RNA corresponding to each sRNA sample could be less). All sRNA-seq libraries created and analyzed in this study are listed in Table S6.

Sequencing libraries

All libraries were analyzed on the Agilent 4150 TapeStation System using D5000 and D1000 ScreenTapes for ChIP-seq/MNase-seq and sRNA-seq samples, respectively. 48 libraries were combined and sequenced on the NextSeq 500 machine (Illumina) using the High Output Kit v2.5 (75 cycles, single-end mode). Typically, 460-500 million indexed reads were generated, corresponding to the average library size of 10 million reads. Raw sequencing data were demultiplexed using bcl2fastq (v2.20) with '--barcode-mismatches 0 --no-lane-splitting' flags. Adapter sequences were removed using cutadapt (v1.15) [75].

Designing custom genome references

Custom genome reference *mNC12* was created by concatenating the following GenBank entries: NC_026614.1, part of M54787.1 encoding the *mat a* locus (3237 bp), NC_026501.1, NC_026502.1, NC_026503.1, NC_026504.1, NC_026505.1, NC_026506.1, NC_026507.1, NW_011929459.1,

NW_011929460.1, NW_011929461.1, NW_011929462.1, NW_011929463.1, NW_011929464.1, NW_011929465.1, NW_011929466.1, NW_011929467.1, NW_011929468.1, NW_011929469.1, NW_011929470.1, NW_011929471.1.

References *mNC12.lacO-tetO* and *mNC12.tetO* (SI Data File 2) were created based on *mNC12* by editing the sequence between *his-3* and *lpl* to reflect the structure of the locus after transformation with pFOC104A and pTSN6, respectively.

Sequence alignment and post-processing

All sequences were aligned to *mNC12.lacO-tetO* as the standard reference. Sequences originating from strains with the lone *tetO* array were also aligned to *mNC12.tetO*, while sequences derived from strains carrying parts of the *lacO* array were aligned to custom genome references that reflected the actual structure of the *his-3–lpl* locus in those strains. Alignment was done using bowtie2 (v2.3.4.1) with a standard set of parameters defined by the '--very-sensitive' option [76]. ChIP-seq/MNase-seq reads were aligned to the genome directly, whereas sRNA-seq reads were first aligned to the *mito_ribo* reference (provided in SI Data File 2), the unaligned reads were retained and aligned to the genome reference. The alignments were post-processed using samtools (v1.7) [77].

Building and analyzing genomic profiles

For each library, a genome profile was constructed by counting the number of reads mapped over a series of non-overlapping 500-bp tiles (defined using the reference *mNC12.lacO-tetO*). Reads were counted using the command 'samtools view -c'. Profiles were normalized by the effective number of reads as follows. For ChIP-seq/MNase-seq samples, the effective number of reads was equal to the total number of reads minus the reads mapped to the mitochondrial genome. For sRNA-seq samples, both mitochondrial and ribosomal reads were subtracted. Profiles of biological replicates were averaged to produce the final profile used for analysis. High-resolution profiles were created using exactly the same approach, except that the tile size was set to 1 bp. For all logarithmic operations to generate scatter plots, a pseudo-count of 1 was added to each each profile value. For computing and plotting physical maps of read-count ratios, only profile values in the denominator were augmented by 1. Matching ChIP-seq 'Input' profiles were used to normalize and plot MNase-seq profiles. All graphs were produced using ggplot2 [78]. Euler diagrams were created using the eulerr R package (v7.0.0, https://CRAN.R-project.org/package=eulerr).

Fluorescence microscopy analysis

Cultures were started by inoculating thawed macroconidia (~10^5 CFUs) into 5 ml of VM medium and grown for 6-7 hours at 30 ºC/160 RPM. For the HU treatment: 38 mg of HU were added to a designated 5-ml culture (for the final concentration of 0.1M), and the culture was incubated for additional 24 hours at 30 ºC/160 RPM.

For all cultures: a 1-ml sample was taken and centrifuged at 10000 ×g, the pellets were collected and spread on glass slides. Images were acquired on an inverted wide-field microscope (Nikon TE2000) equipped with a 100×/1.4 NA immersion objective and a Prime BSI Express sCMOS camera (Teledyne Photometrics) with 6.5×6.5 μm pixel size. A SPECTRA X Light Engine lamp (Lumencor) set to power 50, for 100 ms, was used to illuminate the samples. For each area of interest, stacks of 32 images were obtained, with a z-step of 200 nm. Raw image data are available upon request.

SI FIGURE LEGENDS

Figure S1. Experimental system.

(A) Sequence properties of the *lacO–tetO* reporter are indicated (see text for explanation). Genes conferring resistance to kanamycin (*KmR*) and gentamicin (*GmR*) in *Escherichia coli* are also indicated.

(B) Density of sRNA-seq reads in the 0.8-Mbp genomic region containing the *lacO–tetO* reporter (calculated per 500 bp, per 1 million mapped reads). Absolute and relative densities (corresponding to ratios of sRNA-seq counts) are shown, as indicated (plotted as in Fig. 5E).

(C) Examples of the reference loci used to normalize and compare expression levels of array-derived sRNAs. For the purpose of the analysis, these loci were represented by 500-bp tiles (see text for explanation).

(D) Scatter plots showing genome-wide changes in sRNA expression (analyzed and plotted as in Fig. 1F). Reference loci are shown as light-blue circles. 'Basenko *et al*' sRNA-seq data were published previously [40].

(E) Histogram showing composition of the *N. crassa* genome with respect to GC-content (analyzed using the same array of tiles as in Fig. 1F). AT-rich DNA is characterized by GC-content below 38-40%.

Figure S2. Silencing of the repressor-bound *tetO* array: properties and regulation.

(A) Densities of ChIP-seq and sRNA-seq reads over the *lacO–tetO* reporter and the neighboring genes (analyzed and plotted as in Fig. 1D,E).

(B) Density of ChIP-seq reads over the *lacO–tetO* reporter and the neighboring genes (analyzed and plotted as in Fig. 1D).

(C) Scatter plots showing the relationship between the hH3 occupancy and GC-content (analyzed and plotted as in Fig. 2E).

(D) Scatter plots showing the relationship between changes in H3K9me3 (normalized by their corresponding 'Input' values) and GC-content. Tiles overlapping the *lacO* and the *tetO* arrays are shown as pink and green circles, respectively.

Figure S3. Genome-wide changes in sRNA expression.

(A) Scatter plots showing the relationship between changes in sRNA expression and GC-content (analyzed and plotted as in Fig. 4C). Tiles overlapping the *lacO* and the *tetO* arrays are shown as pink and green circles, respectively.

(B) Density of sRNA-seq reads over the *lacO–tetO* reporter and the neighboring genes (analyzed and plotted as in Fig. 1E). The increased expression of background sRNAs is evidenced by having multiple reads mapped to *his-3* and *lpl*.

(C) Genome-wide changes in sRNA expression (analyzed and plotted as in Fig. 5E).

Figure S4. Fluorescence microscopy analysis of the repressor-bound *tetO* array.

For each area of interest, image stacks were obtained with a z-step of 200 nm (Methods), and a single plane with the brightest localized signal was chosen for display. Images of several representative nuclei are shown for the indicated conditions.

Figure S5. Silencing of the repressor-bound *tetO* array does not require CHD1.

(A) Density of ChIP-seq reads over the *lacO–tetO* reporter and the neighboring genes (analyzed and plotted as in Fig. 1D).

(B) Scatter plot showing genome-wide changes in sRNA expression (analyzed and plotted as in Fig. 1F).

(C) Scatter plot showing the relationship between the hH3 occupancy and GC-content (analyzed and plotted as s in Fig. 2E).

(D) Scatter plots showing the relationship between changes in hH3 occupancy and H3K9me3 versus GC-content (analyzed and plotted as in Fig. S2D).

Figure S6. The role of SAD-6 in chromatin regulation.

(A) Density of sRNA-seq reads over the *lacO–tetO* reporter and the neighboring genes (analyzed and plotted as in Fig. 1E).

(B) Scatter plots showing the relationship between changes in histone occupancy and H3K9me3 versus GC-content (analyzed and plotted as in Fig. S2D).

(C) Scatter plot showing the relationship between changes in MNase sensitivity and GC-content. Tiles overlapping the *lacO* and the *tetO* arrays are shown as pink and green circles, respectively.

(D) Strategy to tag SAD-6 with 3xFLAG (the construct is provided on the plasmid pFOC109N).

(E) Genome-wide changes in sRNA expression (analyzed and plotted as in Fig. 5E).

(F) Genome-wide changes in hH3 occupancy and H3K9me3, calculated as ratios of ChIP-seq reads (the same array of 500-bp tiles was used as in Fig. 1F). Denominator values were augmented by 1.

(G) Genome-wide changes in MNase sensitivity, calculated as ratios of MNase-seq reads (the same array of 500-bp tiles was used as in Fig. 1F). Denominator values were augmented by 1.

(H) Genome-wide changes in FLAG-SAD-6 occupancy (analyzed and plotted as in Fig. S6F).

(I) Region *r1*, in which sRNAs expression is strongly suppressed in the absence of SAD-6.

(J) Region *r2*, in which constitutive heterochromatin is eliminated between two islands of AT-rich DNA in the absence of SAD-6.

(K) Region *r3*, characterized by strong enrichment in FLAG-SAD-6.

Figure S7. MNase-seq analysis of the *tetO* array.

(A) Density of MNase-seq reads over the *tetO* array (analyzed and plotted as in Fig. 1D).

(B) Density of ChIP-seq reads over the *tetO* array (analyzed and plotted as in Fig. 1D).

(C) Density of MNase-seq reads over the *tetO* array (analyzed and plotted as in Fig. 1D).

Figure S8. Starvation-induced silencing of the *tetO* array: properties and regulation.

(A) Densities of ChIP-seq and sRNA-seq reads over the *tetO* array and the neighboring genes (analyzed and plotted as in Fig. 1D,E).

(B) Genome-wide changes in sRNA expression (analyzed and plotted as in Fig. 5E).

(C) Genome-wide changes in hH3 occupancy and H3K9me3 (analyzed and plotted as in Fig. S6F).

(D) Genome-wide changes in MNase sensitivity (analyzed and plotted as in Fig. S6G).

Figure S9. Post-transcriptional silencing of the *lacO* array and AT-rich DNA: properties and regulation.

(A) Densities of ChIP-seq and sRNA-seq reads over the *lacO–tetO* reporter and the neighboring genes (analyzed and plotted as in Fig. 1D,E).

(B) Scatter plots showing genome-wide changes in sRNA expression (analyzed and plotted as in Fig. 1F). Tiles overlapping the *lacO* and the *tetO* arrays are shown as pink and green circles, respectively.

(C) Scatter plot showing the relationship between changes in sRNA expression and GC-content (analyzed and plotted as in Fig. 4C). Tiles overlapping the *lacO* and the *tetO* arrays are shown as pink and green circles, respectively.

(D) Density of sRNA-seq reads over the *lacO–tetO* reporter and the neighboring genes (analyzed and plotted as in Fig. 1E). In the *sad-6Δ* strain (Strain ID: T752.13h, Table S2), the *lacO* array contained a large deletion.

(E) Scatter plots showing the relationship between MNase sensitivity and GC-content (analyzed and plotted as in Fig. 2C).

(F) Scatter plot showing the relationship between changes in sRNA expression (analyzed as in Fig. 4C) and changes in MNase sensitivity (analyzed as in Fig. 2C). AT-rich DNA is defined as in Fig. 5F).

(G) Densities of ChIP-seq and sRNA-seq reads over the *lacO–tetO* reporter and the neighboring genes (analyzed and plotted as in Fig. 1D,E).
(H) Scatter plots showing the relationship between changes in sRNA expression and GC-content (analyzed and plotted as Fig. 4C). Tiles overlapping the *lacO* and the *tetO* arrays are shown as pink and green circles, respectively.
(I) Scatter plots showing the relationship between hH3 occupancy and GC-content (analyzed and plotted as in Fig. 2E).

Figure S10. Assaying genetic stability of the *lacO–tetO* reporter.
(A) Strategy to generate clonal populations of nuclei, in which the stability of the arrays was assayed. Several macroconidial isolates from a primary vegetative culture were tested by multiplex PCR for the presence of the arrays (see text for explanation). A single primary clone with the intact arrays was chosen to start a secondary culture, from which 28 random progeny were selected and re-assayed for the presence of the arrays.
(B) PCR products were resolved on agarose gels. Missing products (corresponding to deletions) are indicated by red rectangles.

Figure S11. Transcriptional and post-transcriptional silencing of the *lacO* array can be decoupled.
(A) A series of isogenic strains was produced with spontaneous deletions in the *lacO* array. In these strains, DIM-5 was either absent (original condition) or present (provided by transformation).
(B) Density of sRNA-seq reads over the *lacO–tetO* reporter and the neighboring genes (analyzed and plotted as in Fig. 1E). Deletions are indicated.
(C) Density of ChIP-seq reads over the *lacO–tetO* reporter and the neighboring genes (analyzed and plotted as in Fig. 1D).
(D) A series of isogenic strains was produced with fragments of the *lacO* array. In these strains, DIM-5 was either absent (original condition) or present (provided by transformation).
(E) Deletions and insertions of the *lacO* array analyzed in this study.
(F) Density of sRNA-seq reads over the *lacO* fragment and the neighboring genes (analyzed as in Fig. 1E).
(G) Density of ChIP-seq reads over the *lacO* fragment and the neighboring genes (analyzed as in Fig. 1D).

SI TABLES

Table S1. *Neurospora* genes analyzed in this study.

Table S2. *Neurospora* strains used in this study.

Table S3. Diagnostic primers used in this study.

Table S4. ChIP-seq libraries created and analyzed in this study.

Table S5. MNase-seq libraries created and analyzed in this study.

Table S6. sRNA-seq libraries created and analyzed in this study.

In Tables S4-S6, the following notations of the culturing conditions were used:

'Tc' - growing cultures were supplemented with 100 µg/µl of tetracycline;

'Bl' - growing cultures were supplemented with 0.1 µg/µl of blasticidin S;

'HU' - pre-grown cultures were incubated for 24 hours in the standard medium supplemented with 0.1M HU;

'no-N' - cultures were shifted to the nitrogen-free medium without HU block;

'N+ control' - cultures were processed analogously to 'no-N' but shifted to the standard (N+) medium instead;

"maintained" - cultures were treated with HU and shifted to the nitrogen-free medium containing HU;

"released" - cultures were treated with HU and shifted to the nitrogen-free medium without HU.

SI DATA FILES

Available at https://figshare.com/s/68987d7763146c2a4e2c; DOI: 10.6084/m9.figshare.24943173

Data File 1. Maps of plasmids used in this study.

Provided as plain-text files in EMBL format, compressed with TAR/GZIP.

Data File 2. Custom genome references used in this study.

Provided as plain-text files in EMBL format, compressed with TAR/GZIP. The following genome references are included: *mNC12.lacO-tetO*, *mNC12.tetO*, and *mito_ribo*.

Data File 3. 500-bp tiles representing reference sRNA-seq loci.

Provided as a plain-text file in CSV format, compressed with TAR/GZIP. Tile coordinates correspond to the genome reference *mNC12.lacO-tetO*.

ADDITIONAL REFERENCES

73. Westergaard, M. and Mitchell, H.K. (1947) Neurospora. V. A synthetic medium favoring sexual reproduction. *American J of Botany* 34, 573–577
74. Gladyshev, E. and Kleckner, N. (2014) Direct recognition of homology between double helices of DNA in Neurospora crassa. *Nat Commun* 5, 3509
75. Martin, M. (2011) Cutadapt removes adapter sequences from high-throughput sequencing reads. *EMBnet j.* 17, 10
76. Langmead, B. and Salzberg, S.L. (2012) Fast gapped-read alignment with Bowtie 2. *Nat Methods* 9, 357–359
77. Danecek, P. *et al.* (2021) Twelve years of SAMtools and BCFtools. *Gigascience* 10, giab008
78. Wickham, H. (2016) *ggplot2: Elegant Graphics for Data Analysis*, Springer-Verlag New York

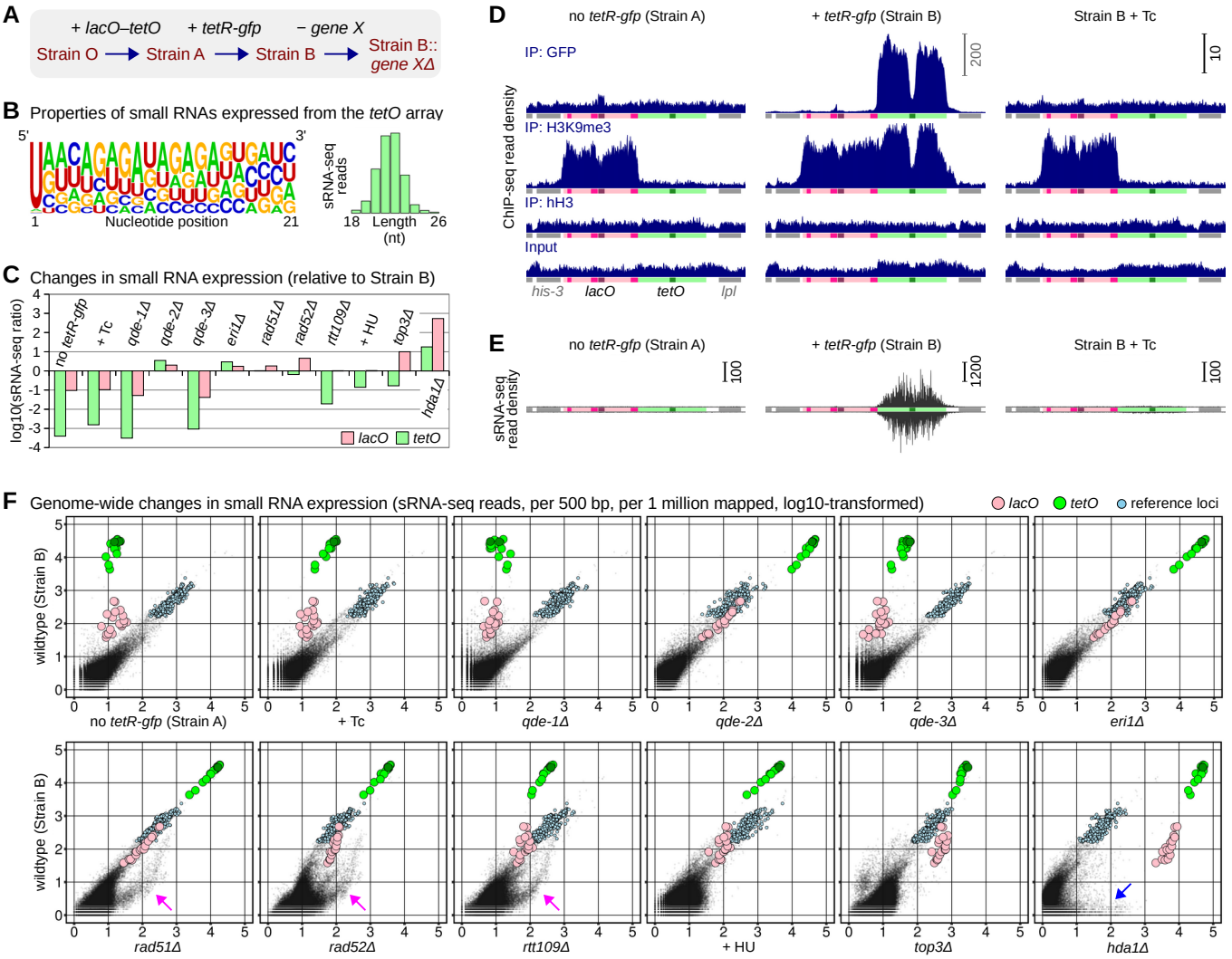
A
+ lacO–tetO
+ tetR-gfp
− gene X
Strain O
Strain A
Strain B
Strain B::
gene XΔ
B Properties of small RNAs expressed from the tetO array
5'
3'
1
Nucleotide position
21
sRNA-seq reads
18
Length (nt)
26
C Changes in small RNA expression (relative to Strain B)
log10(sRNA-seq ratio)
no tetR-gfp
+ Tc
qde-1Δ
qde-2Δ
qde-3Δ
eri1Δ
rad51Δ
rad52Δ
rtt109Δ
+ HU
top3Δ
hda1Δ
lacO
tetO
D
no tetR-gfp (Strain A)
+ tetR-gfp (Strain B)
Strain B + Tc
IP: GFP
IP: H3K9me3
IP: hH3
Input
ChIP-seq read density
200
10
his-3
lacO
tetO
lpl
E
sRNA-seq read density
100
1200
100
F Genome-wide changes in small RNA expression (sRNA-seq reads, per 500 bp, per 1 million mapped, log10-transformed)
lacO
tetO
reference loci
wildtype (Strain B)
no tetR-gfp (Strain A)
+ Tc
qde-1Δ
qde-2Δ
qde-3Δ
eri1Δ
rad51Δ
rad52Δ
rtt109Δ
+ HU
top3Δ
hda1Δ

Figure 1

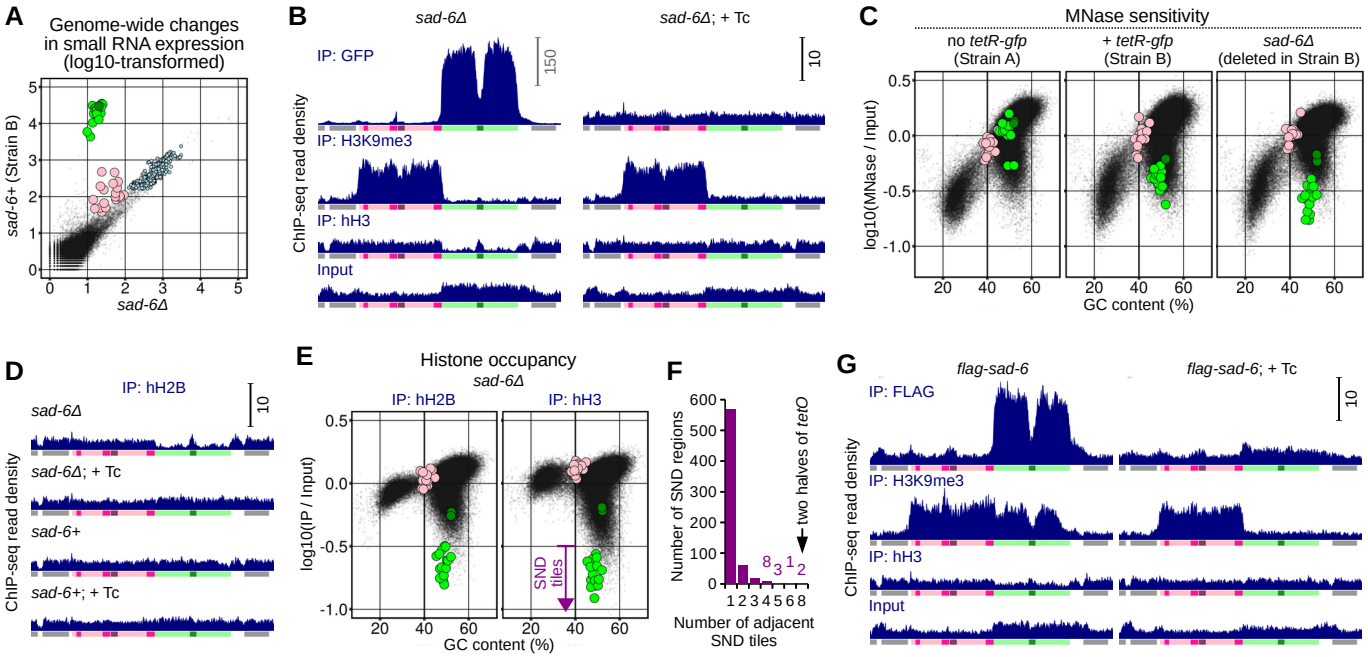
A
Genome-wide changes
in small RNA expression
(log10-transformed)
sad-6+ (Strain B)
sad-6Δ
B
sad-6Δ
sad-6Δ; + Tc
IP: GFP
IP: H3K9me3
IP: hH3
Input
ChIP-seq read density
150
10
C
MNase sensitivity
no tetR-gfp
(Strain A)
+ tetR-gfp
(Strain B)
sad-6Δ
(deleted in Strain B)
log10(MNase / Input)
GC content (%)
D
IP: hH2B
sad-6Δ
sad-6Δ; + Tc
sad-6+
sad-6+; + Tc
ChIP-seq read density
10
E
Histone occupancy
sad-6Δ
IP: hH2B
IP: hH3
log10(IP / Input)
SND
tiles
GC content (%)
F
Number of SND regions
two halves of tetO
Number of adjacent
SND tiles
G
flag-sad-6
flag-sad-6; + Tc
IP: FLAG
IP: H3K9me3
IP: hH3
Input
ChIP-seq read density
10

Figure 2

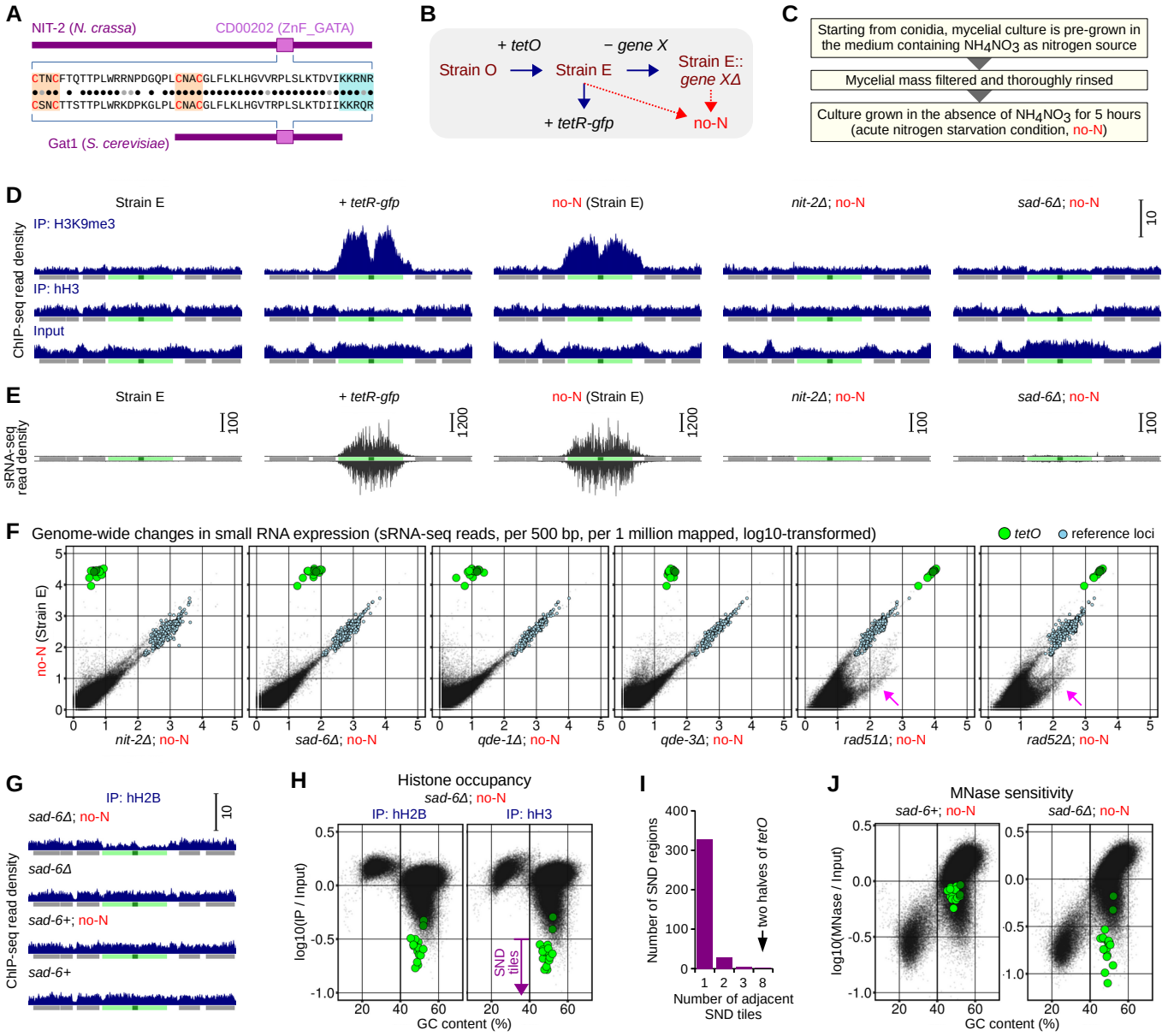
A
NIT-2 (N. crassa)
CD00202 (ZnF_GATA)
CTNCFTQTTPLWRRNPDGQPLCNACGLFLKLHGVVRPLSLKTDVIKKRNR
CSNCTTSTTPLWRKDPKGLPLCNACGLFLKLHGVTRPLSLKTDIIKKRQR
Gat1 (S. cerevisiae)
B
+ tetO
− gene X
Strain O
Strain E
Strain E::
gene XΔ
+ tetR-gfp
no-N
C
Starting from conidia, mycelial culture is pre-grown in the medium containing NH4NO3 as nitrogen source
Mycelial mass filtered and thoroughly rinsed
Culture grown in the absence of NH4NO3 for 5 hours (acute nitrogen starvation condition, no-N)
D
Strain E
+ tetR-gfp
no-N (Strain E)
nit-2Δ; no-N
sad-6Δ; no-N
IP: H3K9me3
IP: hH3
Input
ChIP-seq read density
10
E
sRNA-seq read density
100
1200
F
Genome-wide changes in small RNA expression (sRNA-seq reads, per 500 bp, per 1 million mapped, log10-transformed)
tetO
reference loci
no-N (Strain E)
nit-2Δ; no-N
sad-6Δ; no-N
qde-1Δ; no-N
qde-3Δ; no-N
rad51Δ; no-N
rad52Δ; no-N
G
IP: hH2B
sad-6Δ; no-N
sad-6Δ
sad-6+; no-N
sad-6+
ChIP-seq read density
10
H
Histone occupancy
sad-6Δ; no-N
IP: hH2B
IP: hH3
log10(IP / Input)
SND tiles
GC content (%)
I
Number of SND regions
two halves of tetO
Number of adjacent SND tiles
J
MNase sensitivity
sad-6+; no-N
sad-6Δ; no-N
log10(MNase / Input)
GC content (%)

Figure 3

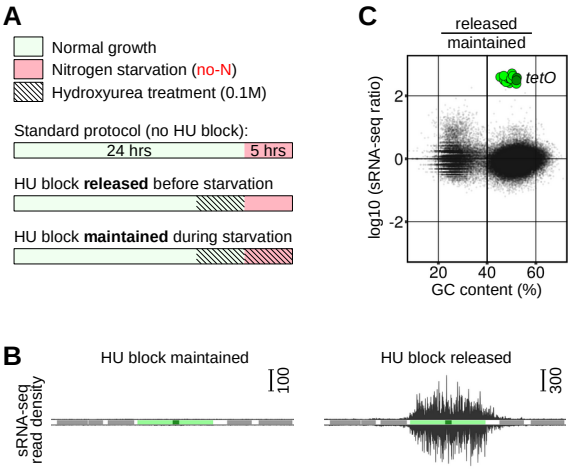
A
Normal growth
Nitrogen starvation (no-N)
Hydroxyurea treatment (0.1M)
Standard protocol (no HU block):
24 hrs
5 hrs
HU block released before starvation
HU block maintained during starvation
C
released
maintained
tetO
log10 (sRNA-seq ratio)
2
0
-2
20
40
60
GC content (%)
B
HU block maintained
HU block released
sRNA-seq
read density
100
300

Figure 4

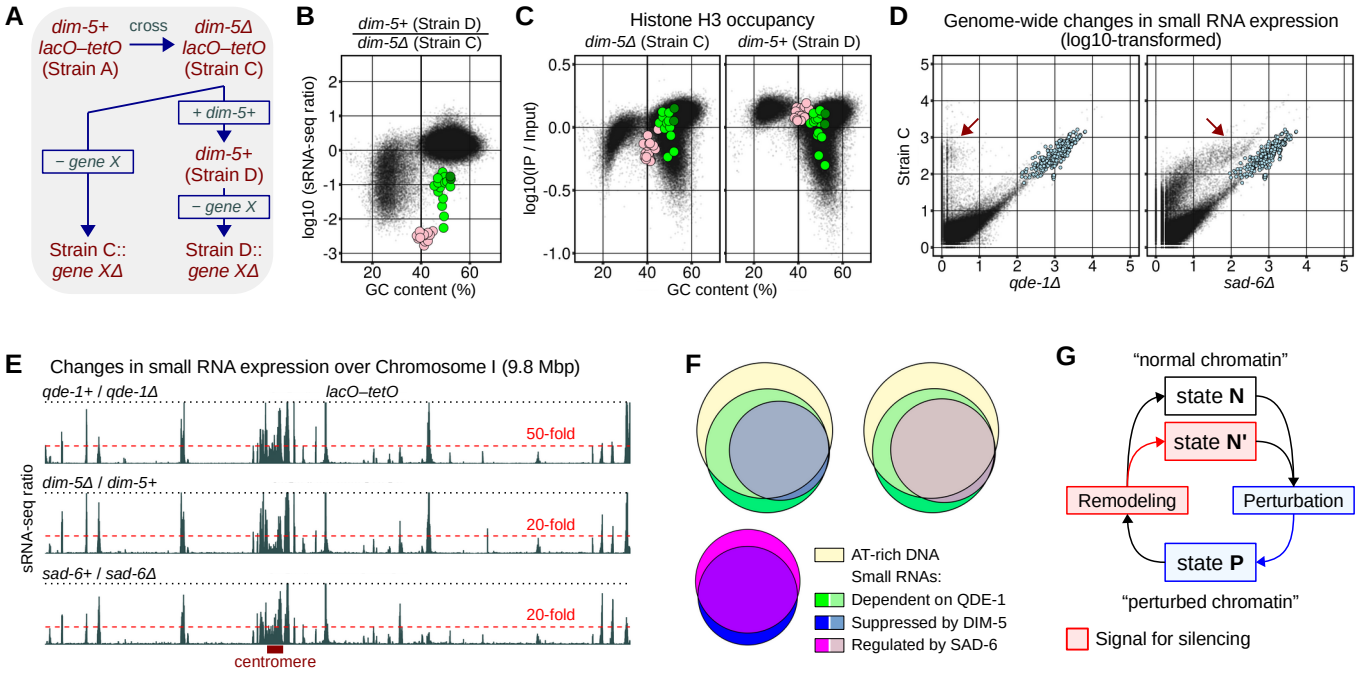
A
dim-5+
lacO–tetO
(Strain A)
cross
dim-5Δ
lacO–tetO
(Strain C)
+ dim-5+
dim-5+
(Strain D)
− gene X
− gene X
Strain C::
gene XΔ
Strain D::
gene XΔ
B
dim-5+ (Strain D)
dim-5Δ (Strain C)
log10 (sRNA-seq ratio)
GC content (%)
C
Histone H3 occupancy
dim-5Δ (Strain C)
dim-5+ (Strain D)
log10(IP / Input)
GC content (%)
D
Genome-wide changes in small RNA expression
(log10-transformed)
Strain C
qde-1Δ
sad-6Δ
E
Changes in small RNA expression over Chromosome I (9.8 Mbp)
qde-1+ / qde-1Δ
lacO–tetO
50-fold
dim-5Δ / dim-5+
20-fold
sad-6+ / sad-6Δ
20-fold
sRNA-seq ratio
centromere
F
AT-rich DNA
Small RNAs:
Dependent on QDE-1
Suppressed by DIM-5
Regulated by SAD-6
G
"normal chromatin"
state N
state N'
Remodeling
Perturbation
state P
"perturbed chromatin"
Signal for silencing

Figure 5

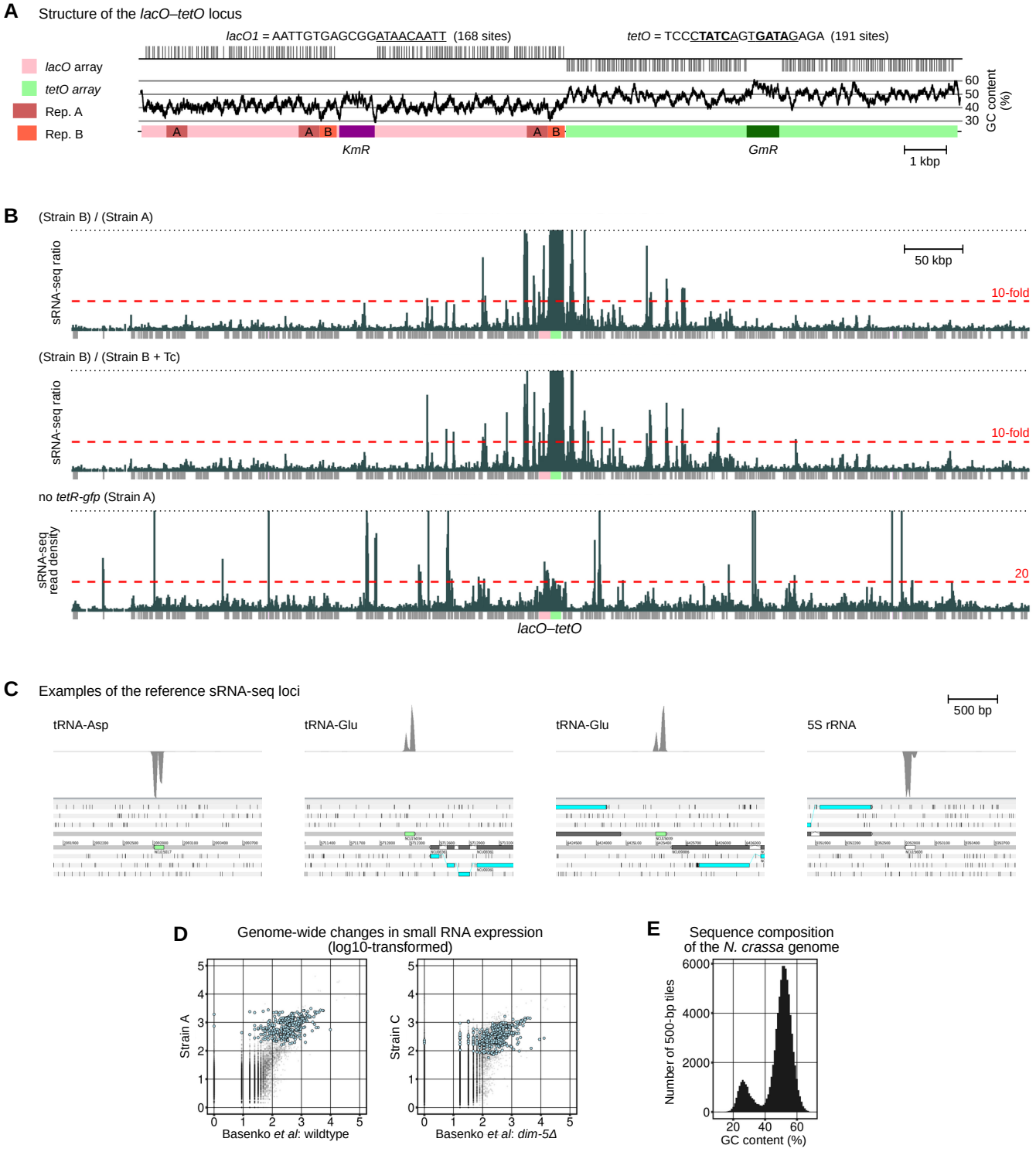
A
Structure of the lacO–tetO locus
lacO1 = AATTGTGAGCGGATAACAATT (168 sites)
tetO = TCCCTATCAGTGATAGAGA (191 sites)
lacO array
tetO array
Rep. A
Rep. B
GC content (%)
KmR
GmR
1 kbp
B
(Strain B) / (Strain A)
sRNA-seq ratio
50 kbp
10-fold
(Strain B) / (Strain B + Tc)
no tetR-gfp (Strain A)
sRNA-seq read density
20
lacO–tetO
C
Examples of the reference sRNA-seq loci
500 bp
tRNA-Asp
tRNA-Glu
tRNA-Glu
5S rRNA
D
Genome-wide changes in small RNA expression (log10-transformed)
Strain A
Basenko et al: wildtype
Strain C
Basenko et al: dim-5Δ
E
Sequence composition of the N. crassa genome
Number of 500-bp tiles
GC content (%)

Figure S1

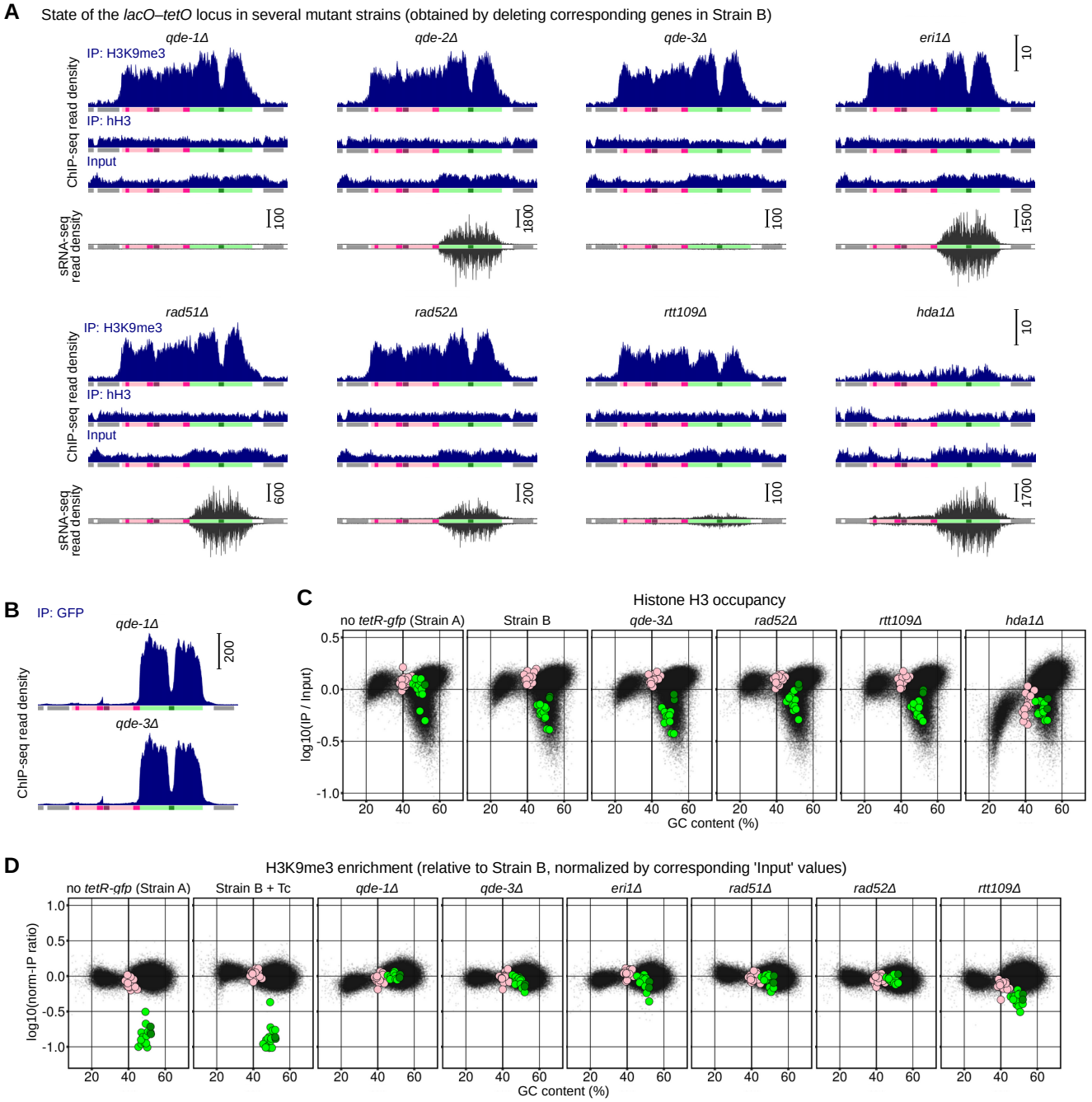
A
State of the lacO–tetO locus in several mutant strains (obtained by deleting corresponding genes in Strain B)
qde-1Δ
qde-2Δ
qde-3Δ
eri1Δ
IP: H3K9me3
IP: hH3
Input
ChIP-seq read density
sRNA-seq read density
rad51Δ
rad52Δ
rtt109Δ
hda1Δ
B
IP: GFP
C
Histone H3 occupancy
no tetR-gfp (Strain A)
Strain B
log10(IP / Input)
GC content (%)
D
H3K9me3 enrichment (relative to Strain B, normalized by corresponding 'Input' values)
Strain B + Tc
log10(norm-IP ratio)

Figure S2

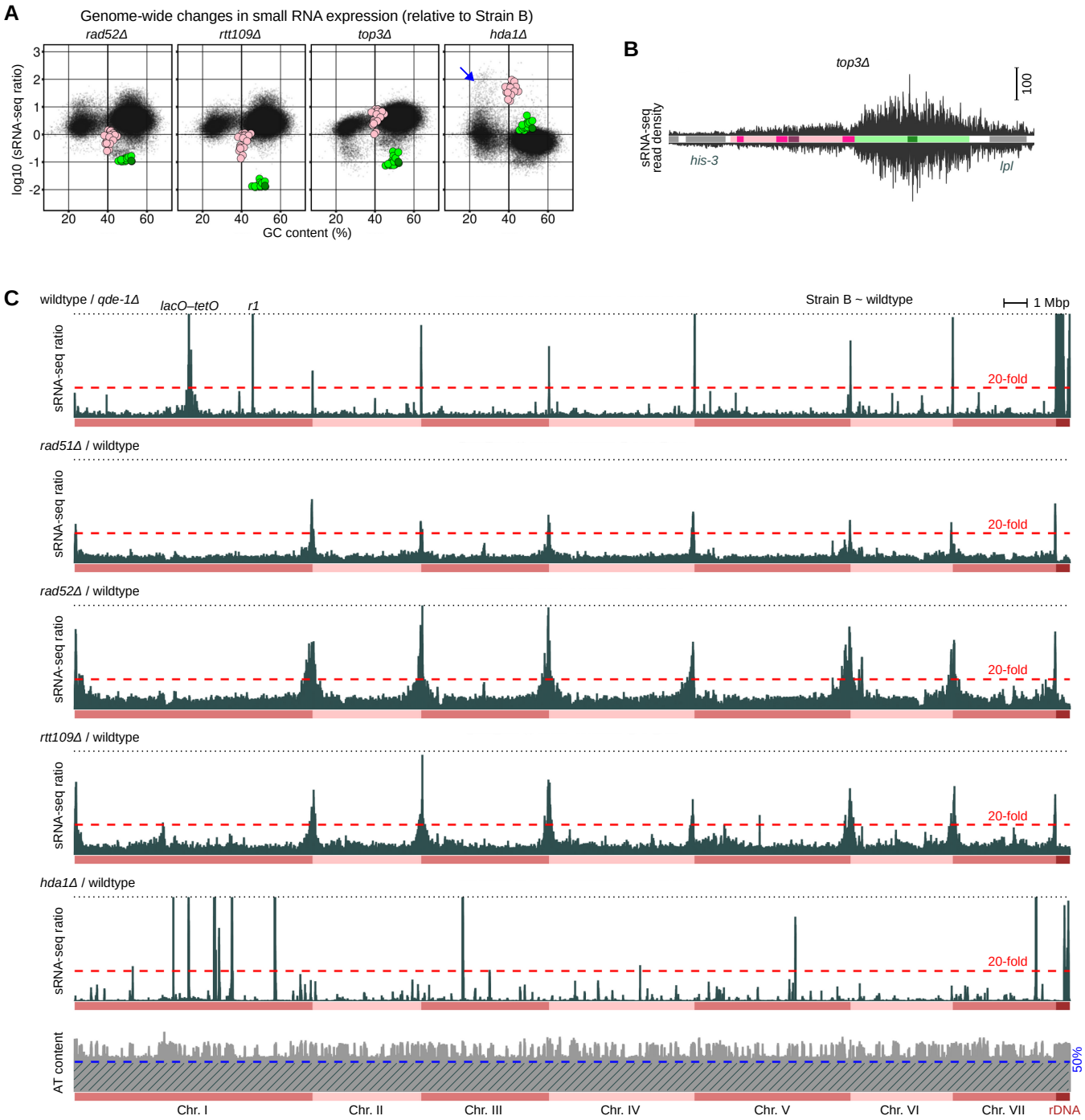
A
Genome-wide changes in small RNA expression (relative to Strain B)
rad52Δ
rtt109Δ
top3Δ
hda1Δ
log10 (sRNA-seq ratio)
GC content (%)
B
top3Δ
100
sRNA-seq read density
his-3
lpl
C
wildtype / qde-1Δ
lacO–tetO
r1
Strain B ~ wildtype
1 Mbp
sRNA-seq ratio
20-fold
rad51Δ / wildtype
rad52Δ / wildtype
rtt109Δ / wildtype
hda1Δ / wildtype
AT content
50%
Chr. I
Chr. II
Chr. III
Chr. IV
Chr. V
Chr. VI
Chr. VII
rDNA

Figure S3

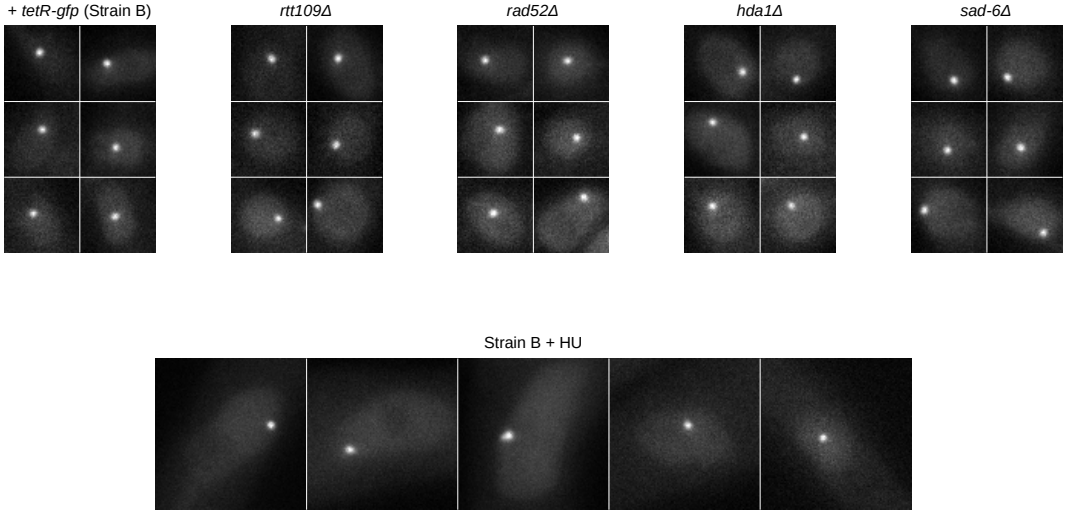

Figure S4

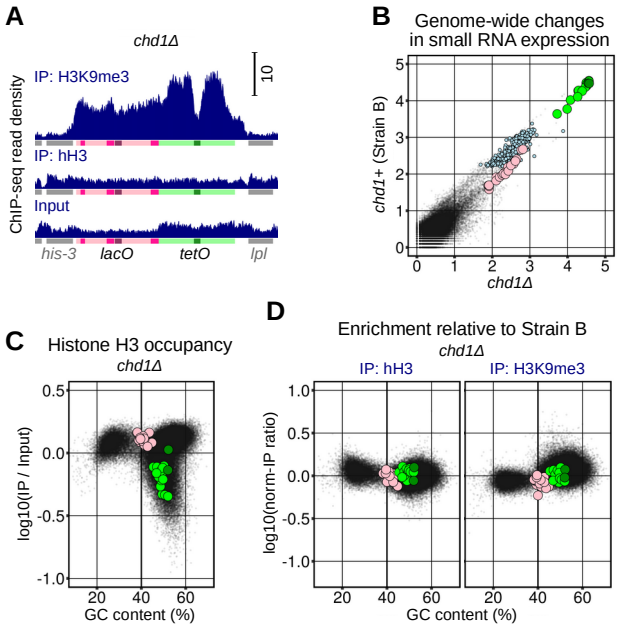
A
chd1Δ
IP: H3K9me3
IP: hH3
Input
ChIP-seq read density
10
his-3
lacO
tetO
lpl
B
Genome-wide changes
in small RNA expression
chd1+ (Strain B)
chd1Δ
C
Histone H3 occupancy
chd1Δ
log10(IP / Input)
GC content (%)
D
Enrichment relative to Strain B
chd1Δ
IP: hH3
IP: H3K9me3
log10(norm-IP ratio)
GC content (%)

Figure S5

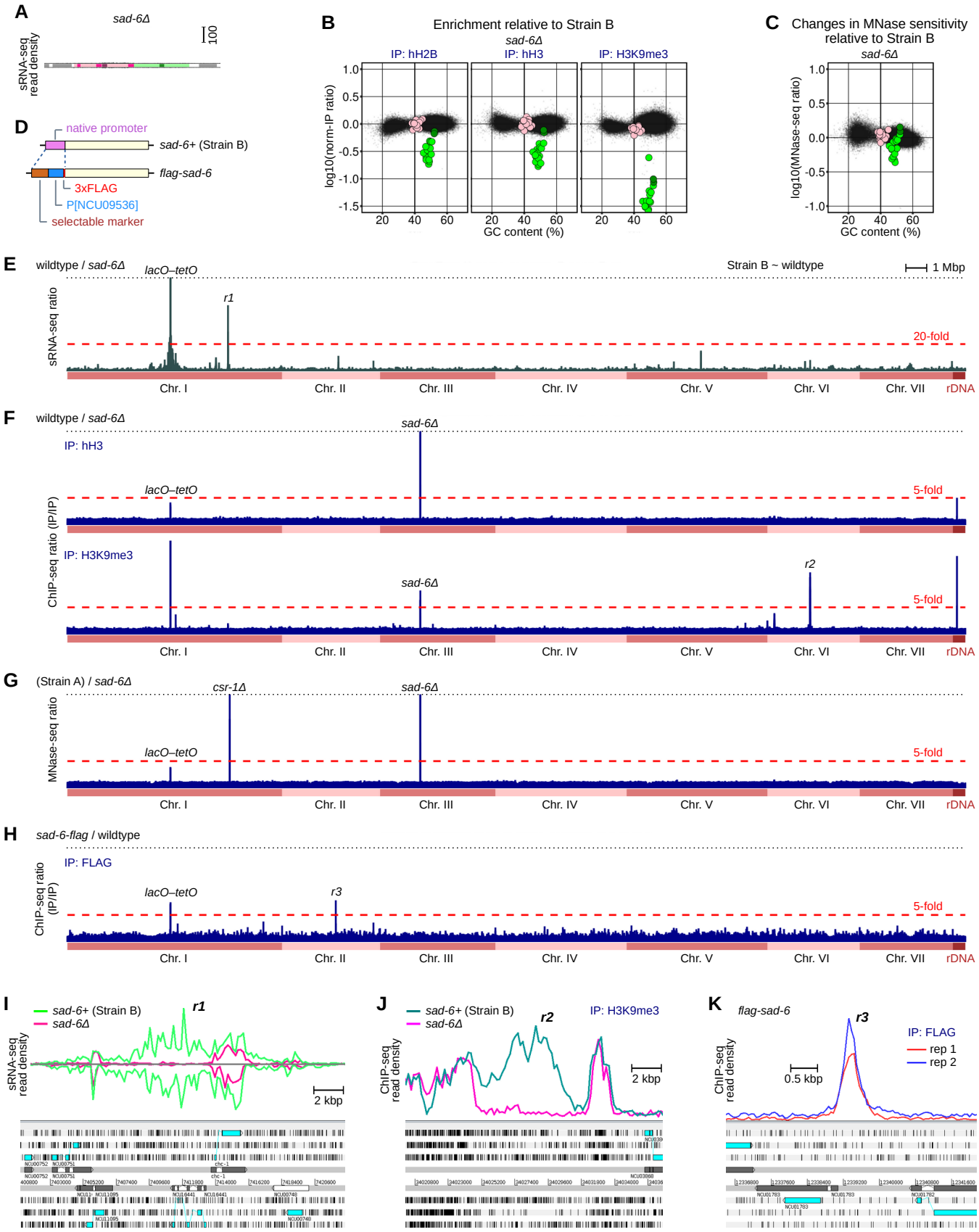
A
sad-6Δ
sRNA-seq read density
100
B
Enrichment relative to Strain B
sad-6Δ
IP: hH2B
IP: hH3
IP: H3K9me3
log10(norm-IP ratio)
GC content (%)
C
Changes in MNase sensitivity relative to Strain B
sad-6Δ
log10(MNase-seq ratio)
GC content (%)
D
native promoter
sad-6+ (Strain B)
flag-sad-6
3xFLAG
P[NCU09536]
selectable marker
E
wildtype / sad-6Δ
lacO–tetO
r1
Strain B ~ wildtype
1 Mbp
sRNA-seq ratio
20-fold
Chr. I
Chr. II
Chr. III
Chr. IV
Chr. V
Chr. VI
Chr. VII
rDNA
F
wildtype / sad-6Δ
sad-6Δ
IP: hH3
lacO–tetO
5-fold
ChIP-seq ratio (IP/IP)
IP: H3K9me3
r2
sad-6Δ
5-fold
G
(Strain A) / sad-6Δ
csr-1Δ
sad-6Δ
MNase-seq ratio
lacO–tetO
5-fold
H
sad-6-flag / wildtype
IP: FLAG
ChIP-seq ratio (IP/IP)
lacO–tetO
r3
5-fold
I
sad-6+ (Strain B)
sad-6Δ
r1
sRNA-seq read density
2 kbp
J
sad-6+ (Strain B)
sad-6Δ
r2
IP: H3K9me3
ChIP-seq read density
2 kbp
K
flag-sad-6
r3
IP: FLAG
rep 1
rep 2
ChIP-seq read density
0.5 kbp

Figure S6

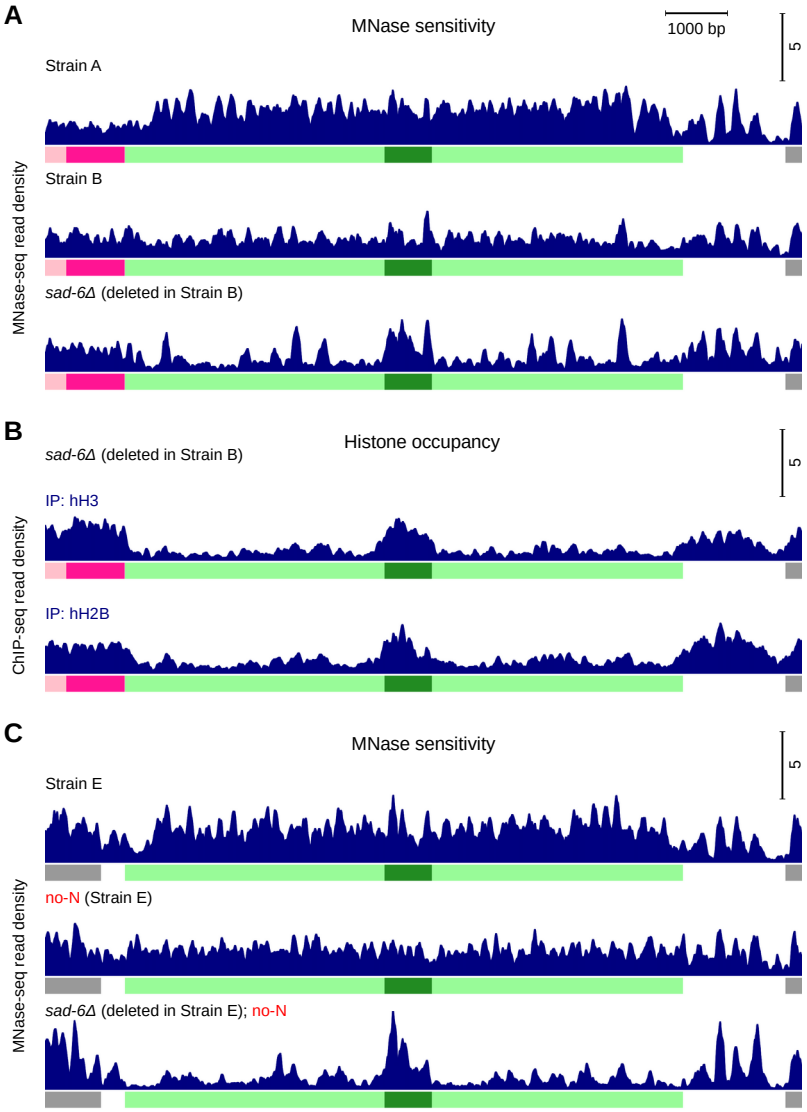
A
MNase sensitivity
1000 bp
5
Strain A
Strain B
sad-6Δ (deleted in Strain B)
MNase-seq read density
B
Histone occupancy
sad-6Δ (deleted in Strain B)
5
IP: hH3
IP: hH2B
ChIP-seq read density
C
MNase sensitivity
5
Strain E
no-N (Strain E)
sad-6Δ (deleted in Strain E); no-N
MNase-seq read density

Figure S7

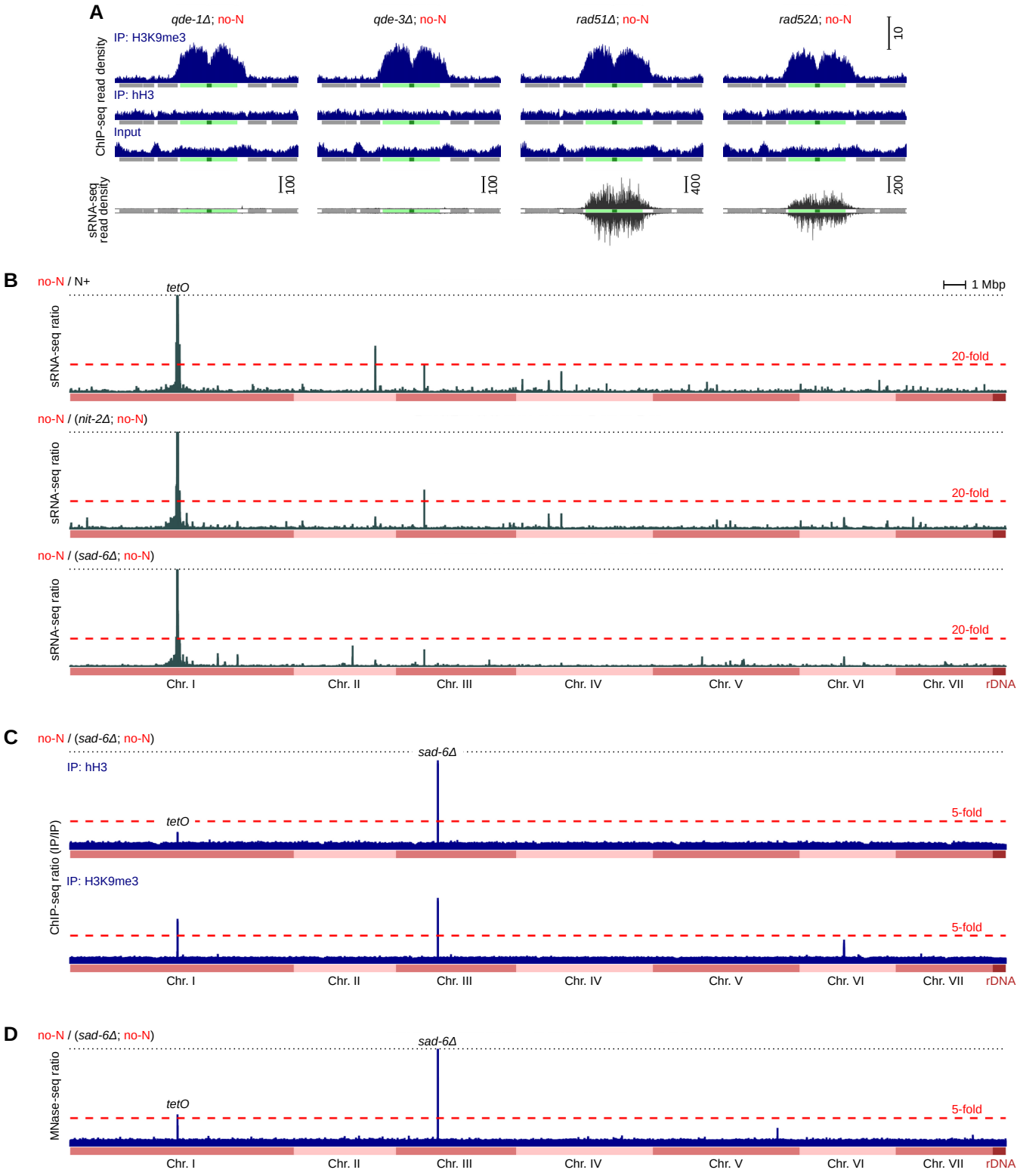
A
qde-1Δ; no-N
qde-3Δ; no-N
rad51Δ; no-N
rad52Δ; no-N
IP: H3K9me3
IP: hH3
Input
ChIP-seq read density
sRNA-seq read density
10
100
100
400
200
B
no-N / N+
tetO
1 Mbp
sRNA-seq ratio
20-fold
no-N / (nit-2Δ; no-N)
no-N / (sad-6Δ; no-N)
Chr. I
Chr. II
Chr. III
Chr. IV
Chr. V
Chr. VI
Chr. VII
rDNA
C
sad-6Δ
IP: hH3
5-fold
IP: H3K9me3
ChIP-seq ratio (IP/IP)
D
MNase-seq ratio

Figure S8

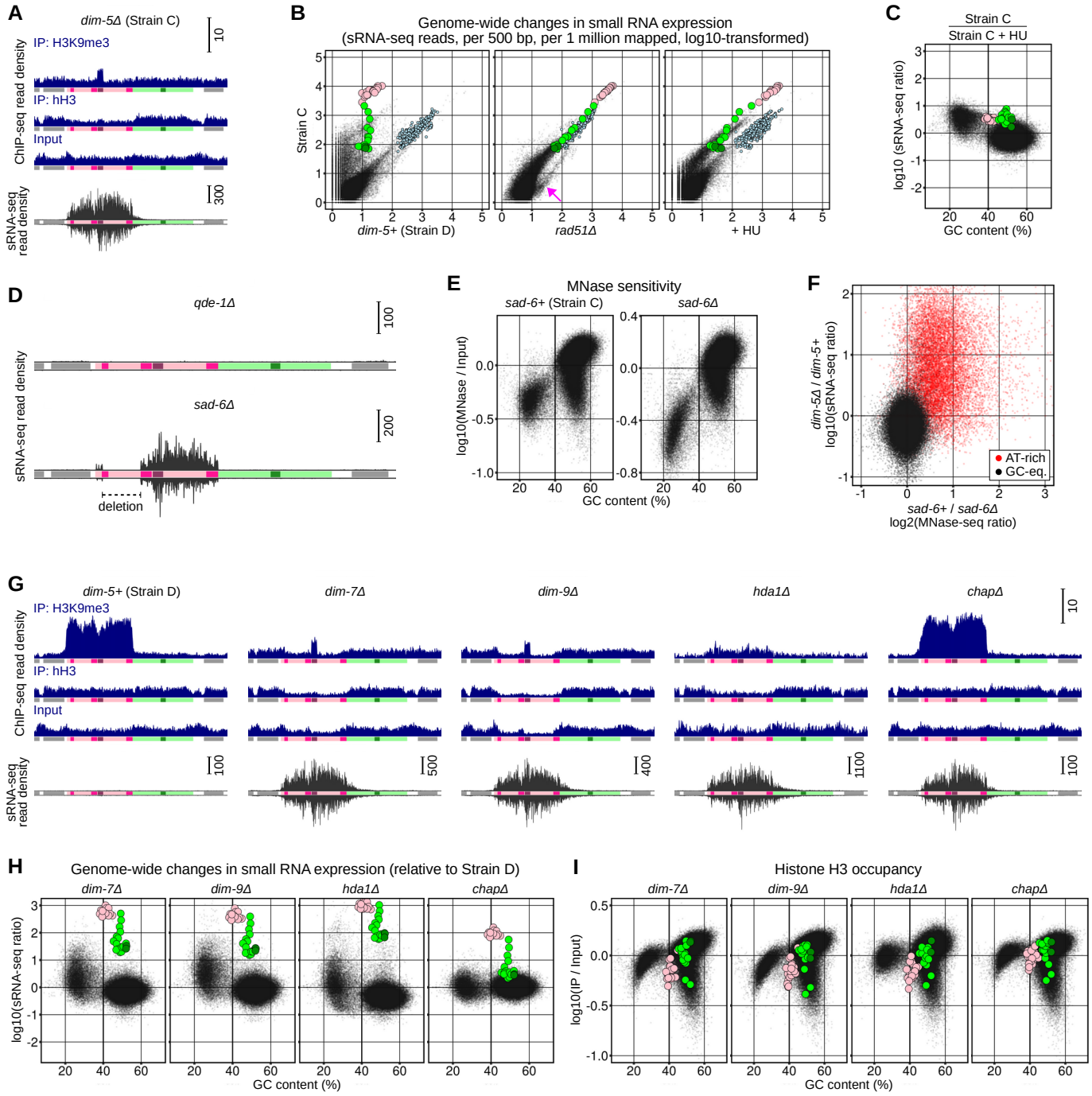
A
dim-5Δ (Strain C)
IP: H3K9me3
IP: hH3
Input
ChIP-seq read density
sRNA-seq read density
B
Genome-wide changes in small RNA expression
(sRNA-seq reads, per 500 bp, per 1 million mapped, log10-transformed)
Strain C
dim-5+ (Strain D)
rad51Δ
+ HU
C
Strain C
Strain C + HU
log10 (sRNA-seq ratio)
GC content (%)
D
qde-1Δ
sad-6Δ
deletion
E
MNase sensitivity
sad-6+ (Strain C)
sad-6Δ
log10(MNase / Input)
GC content (%)
F
dim-5Δ / dim-5+
log10(sRNA-seq ratio)
AT-rich
GC-eq.
sad-6+ / sad-6Δ
log2(MNase-seq ratio)
G
dim-5+ (Strain D)
dim-7Δ
dim-9Δ
hda1Δ
chapΔ
IP: H3K9me3
IP: hH3
Input
ChIP-seq read density
sRNA-seq read density
H
Genome-wide changes in small RNA expression (relative to Strain D)
dim-7Δ
dim-9Δ
hda1Δ
chapΔ
log10(sRNA-seq ratio)
GC content (%)
I
Histone H3 occupancy
dim-7Δ
dim-9Δ
hda1Δ
chapΔ
log10(IP / Input)
GC content (%)

Figure S9

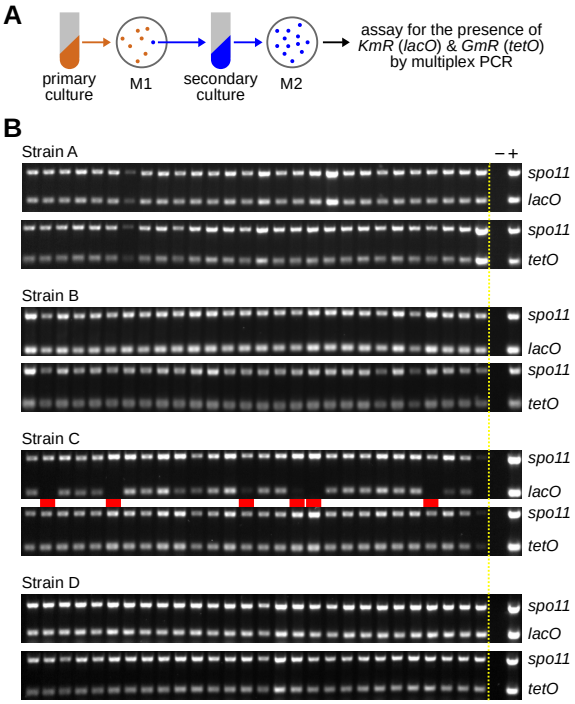
A
primary culture
M1
secondary culture
M2
assay for the presence of KmR (lacO) & GmR (tetO) by multiplex PCR
B
Strain A
− +
spo11
lacO
spo11
tetO
Strain B
spo11
lacO
spo11
tetO
Strain C
spo11
lacO
spo11
tetO
Strain D
spo11
lacO
spo11
tetO

Figure S10

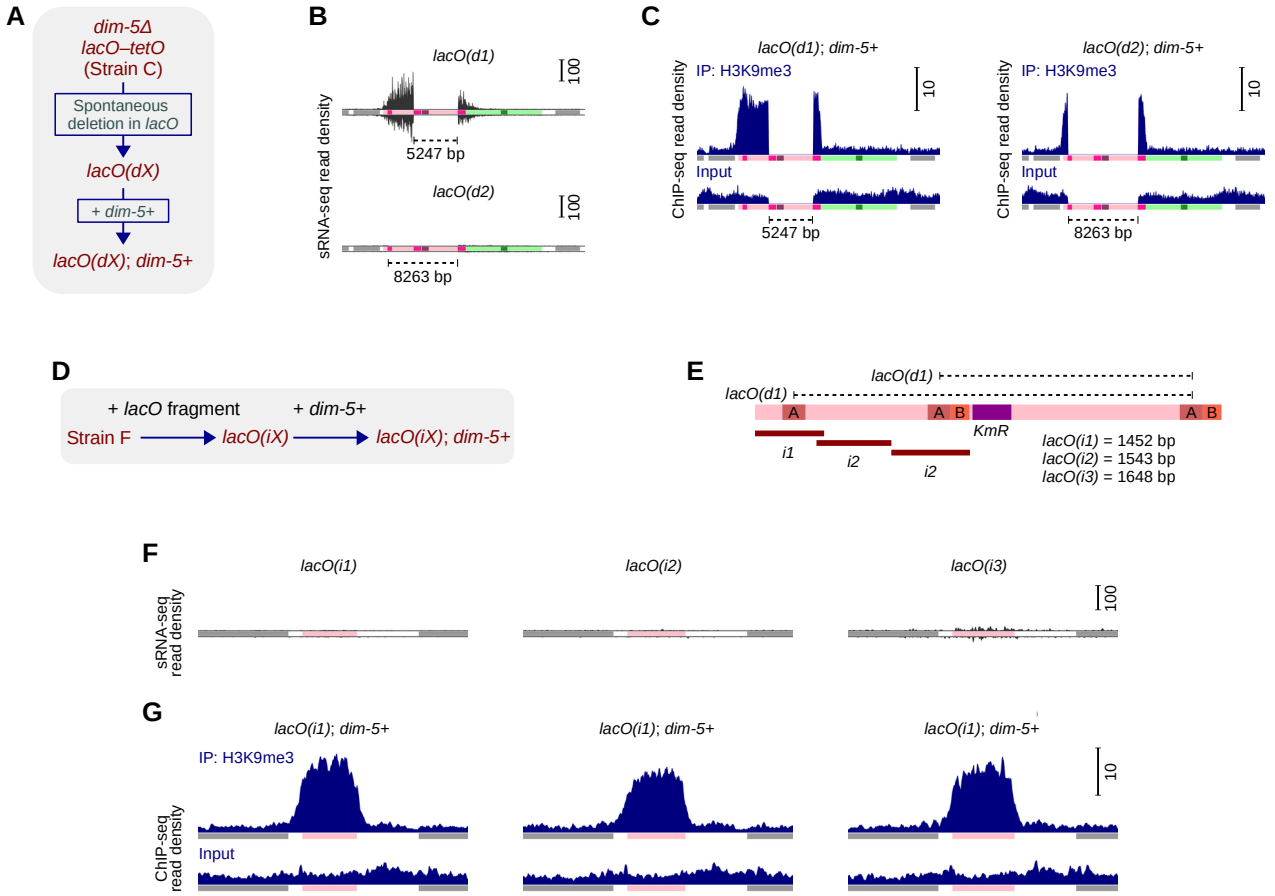
A
dim-5Δ
lacO–tetO
(Strain C)
Spontaneous deletion in lacO
lacO(dX)
+ dim-5+
lacO(dX); dim-5+
B
lacO(d1)
100
sRNA-seq read density
5247 bp
lacO(d2)
100
8263 bp
C
lacO(d1); dim-5+
IP: H3K9me3
10
ChIP-seq read density
Input
5247 bp
lacO(d2); dim-5+
IP: H3K9me3
10
ChIP-seq read density
Input
8263 bp
D
+ lacO fragment
+ dim-5+
Strain F
lacO(iX)
lacO(iX); dim-5+
E
lacO(d1)
lacO(d1)
A
A B
A B
KmR
i1
i2
i2
lacO(i1) = 1452 bp
lacO(i2) = 1543 bp
lacO(i3) = 1648 bp
F
lacO(i1)
lacO(i2)
lacO(i3)
sRNA-seq read density
100
G
lacO(i1); dim-5+
lacO(i1); dim-5+
lacO(i1); dim-5+
IP: H3K9me3
10
ChIP-seq read density
Input

Figure S11

Table S1. *Neurospora* genes analyzed in this study.

Gene	Standard name	Linkage group	Protein accession	Full name	Synonym (if any)
chap	NCU01796	II	XP_956474.1	*CDP−2- and HDA1 associating protein*	
chd1	NCU03060	I	XP_011393066.1	*chromatin remodeling factor 6-1*	*crf6-1*
csr−1	NCU00726	I	XP_011392822.1	*cyclosporin-resistant−1*	*cyp*
dim−2	NCU02247	VII	XP_959891.1	*defective in methylation−2*	
dim−5	NCU04402	IV	XP_957479.2	*defective in methylation−5*	*Su(var)3-9*
dim−7	NCU04152	V	XP_961308.2	*defective in methylation−7*	
dim−9	NCU01656	II	XP_956278.3	*defective in methylation−9*	
eri1	NCU06684	V	XP_011394691.1	*RNA binding protein*	
hda1	NCU01525	II	XP_956974.3	*histone deacetylase−1*	
hh2b	NCU02435	VII	XP_959440.1	*histone H2B*	
hh3	NCU01635	II	XP_956003.1	*histone H3*	
his−3	NCU03139	I	XP_964188.1	*histidine−3*	
lpl	NCU03141	I	XP_964190.2	*lysophospholipase*	
mus−52	NCU00077	III	XP_956387.3	*mutagen sensitive−52*	*KU80*
nit−2	NCU09068	I	XP_963796.3	*nitrate nonutilizer−2*	*areA*
qde−1	NCU07534	III	XP_959047.1	*quelling-defective−1*	
qde−2	NCU04730	VI	XP_011394903.1	*quelling-defective−2*	
qde−3	NCU08598	I	XP_964030.3	*quelling-defective−3*	*mus−19*
rad51	NCU02741	I	XP_965126.1	*meiotic−3*	*mei−3*
rad52	NCU04275	V	XP_961065.2	*mutagen sensitive−11*	*mus−11*
rid	NCU02034	I	XP_011392925.1	*RIP defective*	
rtt109	NCU09825	V	XP_958524.1	*DNA damage response protein Rtt109*	
sad−6	NCU06190	III	XP_963002.3	*atrx ortholog*	*ATRX*
set−7	NCU07496	I	XP_965043.2	*SET-domain histone methyltransferase−7*	*E(z)*
spo11	NCU01120	V	XP_961027.3	*spo11 ortholog*	
top3	NCU00081	III	XP_956391.3	*DNA topoisomerase 3-beta*	

Table S2. *Neurospora* strains used in this study.

Genetic condition	Strain ID	Genotype	Source
Strain O	C58.7	*a; ridΔ; dim−2Δ; mus−52Δ; his−3*	ref. 16
Strain A	T647.1h	*a; ridΔ; dim−2Δ; mus−52Δ; his−3+::lacO−tetO*	C58.7 transformed with pFOC104A
Strain B	T658.1	*a; ridΔ; dim−2Δ; mus−52Δ; his−3+::lacO−tetO; csr−1::tetR−gfp*	T647.1h transformed with pTSN7B
Strain B::chd1Δ	T709.3h	*a; ridΔ; dim−2Δ; mus−52Δ; his−3+::lacO−tetO; csr−1::tetR−gfp; chd1Δ*	T658.1 transformed with pFOC111B
Strain B::eri1Δ	T770.2h	*a; ridΔ; dim−2Δ; mus−52Δ; his−3+::lacO−tetO; csr−1::tetR−gfp; eri1Δ*	T658.1 transformed with pSCR8B
Strain B::hda1Δ	T714.8h	*a; ridΔ; dim−2Δ; mus−52Δ; his−3+::lacO−tetO; csr−1::tetR−gfp; hda1Δ*	T658.1 transformed with pFOC121B
Strain B::qde−1Δ	T710.2h	*a; ridΔ; dim−2Δ; mus−52Δ; his−3+::lacO−tetO; csr−1::tetR−gfp; qde−1Δ*	T658.1 transformed with pFOC120B
Strain B::qde−2Δ	T711.21h	*a; ridΔ; dim−2Δ; mus−52Δ; his−3+::lacO−tetO; csr−1::tetR−gfp; qde−2Δ*	T658.1 transformed with pFOC113B
Strain B::qde−3Δ	T712.2h	*a; ridΔ; dim−2Δ; mus−52Δ; his−3+::lacO−tetO; csr−1::tetR−gfp; qde−3Δ*	T658.1 transformed with pFOC114B
Strain B::rad51Δ	T737.1h	*a; ridΔ; dim−2Δ; mus−52Δ; his−3+::lacO−tetO; csr−1::tetR−gfp; rad51Δ*	T658.1 transformed with pFOC106B
Strain B::rad52Δ	T738.1h	*a; ridΔ; dim−2Δ; mus−52Δ; his−3+::lacO−tetO; csr−1::tetR−gfp; rad52Δ*	T658.1 transformed with pFOC107B
Strain B::rtt109Δ	T786.3h	*a; ridΔ; dim−2Δ; mus−52Δ; his−3+::lacO−tetO; csr−1::tetR−gfp; rtt109Δ*	T658.1 transformed with pFOC129B
Strain B::sad−6Δ	T707.51h	*a; ridΔ; dim−2Δ; mus−52Δ; his−3+::lacO−tetO; csr−1::tetR−gfp; sad−6Δ*	T658.1 transformed with pFOC109B
Strain B::flag−sad−6	T827.7h	*a; ridΔ; dim−2Δ; mus−52Δ; his−3+::lacO−tetO; csr−1::tetR−gfp; flag−sad−6*	T658.1 transformed with pFOC109N
Strain B::top3Δ	T812.11h	*a; ridΔ; dim−2Δ; mus−52Δ; his−3+::lacO−tetO; csr−1::tetR−gfp; top3Δ*	T658.1 transformed with pSCR12B
Strain E	T601.2h	*a; ridΔ; dim−2Δ; mus−52Δ; his−3+::tetO*	C58.7 transformed with pTSN6
Strain E::tetR−gfp	T753.1	*a; ridΔ; dim−2Δ; mus−52Δ; his−3+::tetO; csr−1::tetR−gfp*	T601.2h transformed with pTSN7B
Strain E::nit−2Δ	T851.1h	*a; ridΔ; dim−2Δ; mus−52Δ; his−3+::tetO; nit−2Δ*	T601.2h transformed with pEAG276B
Strain E::qde−1Δ	T839.10h	*a; ridΔ; dim−2Δ; mus−52Δ; his−3+::tetO; qde−1Δ*	T601.2h transformed with pFOC120B
Strain E::qde−3Δ	T840.10h	*a; ridΔ; dim−2Δ; mus−52Δ; his−3+::tetO; qde−3Δ*	T601.2h transformed with pFOC114B
Strain E::rad51Δ	T847.3h	*a; ridΔ; dim−2Δ; mus−52Δ; his−3+::tetO; rad51Δ*	T601.2h transformed with pFOC106B
Strain E::rad52Δ	T848.1h	*a; ridΔ; dim−2Δ; mus−52Δ; his−3+::tetO; rad52Δ*	T601.2h transformed with pFOC107B
Strain E::sad−6Δ	T774.4h	*a; ridΔ; dim−2Δ; mus−52Δ; his−3+::tetO; sad−6Δ*	T601.2h transformed with pFOC109B
Strain G	C252.1	*A; ridΔ; dim−2Δ; dim−5Δ; set−7Δ; sad−2Δ*	Cross progeny of C205.11 & C244.9
Strain C	C290.6	*A; ridΔ; dim−2Δ; dim−5Δ; set−7Δ; mus−52Δ; his−3+::lacO−tetO*	Cross progeny of T647.1h & C252.1
Strain C::lacO(d1)	C290.6.C4	*A; ridΔ; dim−2Δ; dim−5Δ; set−7Δ; mus−52Δ; his−3+::lacO(d1)−tetO*	Clonal isolate of C290.6
Strain C::lacO(d2)	C290.6.C6	*A; ridΔ; dim−2Δ; dim−5Δ; set−7Δ; mus−52Δ; his−3+::lacO(d2)−tetO*	Clonal isolate of C290.6
Strain C::lacO(d1); dim−5+	T697.1	*A; ridΔ; dim−2Δ; dim−5Δ; set−7Δ; mus−52Δ; his−3+::lacO(d1)−tetO; csr−1::dim−5+*	C290.6.C4 transformed with pEAG247A
Strain C::lacO(d2); dim−5+	T698.1	*A; ridΔ; dim−2Δ; dim−5Δ; set−7Δ; mus−52Δ; his−3+::lacO(d2)−tetO; csr−1::dim−5+*	C290.6.C6 transformed with pEAG247A
Strain C::dim−5+	T663.2	*A; ridΔ; dim−2Δ; dim−5Δ; set−7Δ; mus−52Δ; his−3+::lacO−tetO; csr−1::dim−5+*	C290.6 transformed with pEAG247A (Strain D)
Strain C::qde−1Δ	T739.4h	*A; ridΔ; dim−2Δ; dim−5Δ; set−7Δ; mus−52Δ; his−3+::lacO−tetO; qde−1Δ*	C290.6 transformed with pFOC120B
Strain C::rad51Δ	T678.5h	*A; ridΔ; dim−2Δ; dim−5Δ; set−7Δ; mus−52Δ; his−3+::lacO−tetO; rad51Δ*	C290.6 transformed with pFOC106B
Strain C::sad−6Δ	T752.13h	*A; ridΔ; dim−2Δ; dim−5Δ; set−7Δ; mus−52Δ; his−3+::lacO−tetO; sad−6Δ*	C290.6 transformed with pFOC109B
Strain D::chapΔ	T690.1h	*A; ridΔ; dim−2Δ; dim−5Δ; set−7Δ; mus−52Δ; his−3+::lacO−tetO; csr−1::dim−5+; chapΔ*	T663.2 transformed with pFOC118B
Strain D::dim−7Δ	T688.2h	*A; ridΔ; dim−2Δ; dim−5Δ; set−7Δ; mus−52Δ; his−3+::lacO−tetO; csr−1::dim−5+; dim−7Δ*	T663.2 transformed with pFOC116B
Strain D::dim−9Δ	T689.2h	*A; ridΔ; dim−2Δ; dim−5Δ; set−7Δ; mus−52Δ; his−3+::lacO−tetO; csr−1::dim−5+; dim−9Δ*	T663.2 transformed with pFOC117B
Strain D::hda1Δ	T743.3h	*A; ridΔ; dim−2Δ; dim−5Δ; set−7Δ; mus−52Δ; his−3+::lacO−tetO; csr−1::dim−5+; hda1Δ*	T663.2 transformed with pFOC121B
Strain F	C146.1	*a; ridΔ; dim−5Δ; set−7Δ; mus−52Δ; his−3*	ref. 16
Strain F::lacO(i1)	T724.2h	*a; ridΔ; dim−5Δ; set−7Δ; mus−52Δ; his−3+::lacO(i1)*	C146.1 transformed with pFOC125A
Strain F::lacO(i2)	T726.1h	*a; ridΔ; dim−5Δ; set−7Δ; mus−52Δ; his−3+::lacO(i2)*	C146.1 transformed with pFOC125C
Strain F::lacO(i3)	T728.1h	*a; ridΔ; dim−5Δ; set−7Δ; mus−52Δ; his−3+::lacO(i3)*	C146.1 transformed with pFOC125E
Strain F::lacO(i1); dim−5+	T764.1	*a; ridΔ; dim−5Δ; set−7Δ; mus−52Δ; his−3+::lacO(i1); csr−1::dim−5+*	T724.2h transformed with pEAG247A
Strain F::lacO(i2); dim−5+	T766.1	*a; ridΔ; dim−5Δ; set−7Δ; mus−52Δ; his−3+::lacO(i2); csr−1::dim−5+*	T726.1h transformed with pEAG247A
Strain F::lacO(i3); dim−5+	T776.1	*a; ridΔ; dim−5Δ; set−7Δ; mus−52Δ; his−3+::lacO(i3); csr−1::dim−5+*	T728.1h transformed with pEAG247A

Table S3. Diagnostic primers used in this study.

Primer name	Internal ID	Sequence
P1	HIS3_F4.2	GTGGATGTCACAATGTCCCT
P2	KMR_F1	ACATGGCAAAGGTAGCGTTG
P3	KMR_R1	TTCCGACTCGTCCAACATCA
P4	F104A_SEQ12	CAATTCGCGGCACAACTCTA
P5	F104A_SEQ14	TCTAGCAAGAGTGGGGATCC
P6	P62_SEQ3	TATAGAGAGCCACTGCGGGA
P7	P62_SEQ4	CCGTGGGTCGATGTTTGATG
P8	HIS3_R7	AGCGAACGAAACCCCTGAAAC
P9	SPO11_F	GTGTCGGAAGTCCCATTACCA
P10	SPO11_R	GTGACGCTGTGTAGTCGCTTG

Table S4. ChIP-seq libraries created and analyzed in this study.

#	Genetic condition	Strain ID	Library	IP (or Input)	Alignment rate (%)	Aligned reads *	Input library	Additional conditions
1	Strain A	T647.1h	CD397_i17_A	GFP	98.3	7929410	CD394_i14_A	
2	Strain A	T647.1h	CD593_i44_A	GFP	87.2	8976252	CD590_i48_A	
3	Strain A	T647.1h	CD2_i3_A	H3K9me3	96.5	5257486	CD1_i1_A	
4	Strain A	T647.1h	CD396_i16_A	H3K9me3	97.4	7609395	CD394_i14_A	
5	Strain A	T647.1h	CD8_i5_A	hH3	99.0	7766288	CD1_i1_A	
6	Strain A	T647.1h	CD395_i15_A	hH3	98.9	7798269	CD394_i14_A	
7	Strain A	T647.1h	CD1_i1_A	Input	99.0	5636932	N/A	
8	Strain A	T647.1h	CD394_i14_A	Input	99.0	8815831	N/A	
9	Strain A	T647.1h	CD590_i48_A	Input	99.0	11094748	N/A	
10	Strain B	T658.1	CD669_i48_A	FLAG	96.2	8815307	CD529_i11_A	
11	Strain B	T658.1	CD671_i47_A	FLAG	96.7	10365761	CD594_i27_A	
12	Strain B	T658.1	CD463_i8_A	GFP	97.3	8909320	CD459_i43_A	Tc
13	Strain B	T658.1	CD477_i10_A	GFP	98.7	6396447	CD473_i5_A	Tc
14	Strain B	T658.1	CD28_i19_A	GFP	96.9	10006244	CD26_i17_A	
15	Strain B	T658.1	CD221_i6_A	GFP	93.1	4276945	CD220_i5_A	
16	Strain B	T658.1	CD461_i45_A	H3K9me3	97.3	8697139	CD459_i43_A	Tc
17	Strain B	T658.1	CD475_i7_A	H3K9me3	97.2	6597607	CD473_i5_A	Tc
18	Strain B	T658.1	CD29_i20_A	H3K9me3	97.6	10922524	CD26_i17_A	
19	Strain B	T658.1	CD92_i43_A	H3K9me3	96.9	7653828	CD89_i40_A	
20	Strain B	T658.1	CD731_i26_A	hH2B	99.0	9636938	CD459_i43_A	Tc
21	Strain B	T658.1	CD732_i27_A	hH2B	99.0	9454969	CD473_i5_A	Tc
22	Strain B	T658.1	CD729_i24_A	hH2B	98.8	9106248	CD529_i11_A	
23	Strain B	T658.1	CD730_i25_A	hH2B	99.0	9851625	CD594_i27_A	
24	Strain B	T658.1	CD460_i44_A	hH3	98.8	11649989	CD459_i43_A	Tc
25	Strain B	T658.1	CD474_i6_A	hH3	99.0	6252061	CD473_i5_A	Tc
26	Strain B	T658.1	CD27_i18_A	hH3	99.0	7549064	CD26_i17_A	
27	Strain B	T658.1	CD90_i41_A	hH3	98.8	7775513	CD89_i40_A	
28	Strain B	T658.1	CD459_i43_A	Input	99.1	15466837	N/A	Tc
29	Strain B	T658.1	CD473_i5_A	Input	99.0	10379300	N/A	Tc
30	Strain B	T658.1	CD26_i17_A	Input	99.0	6046340	N/A	
31	Strain B	T658.1	CD89_i40_A	Input	98.9	8480540	N/A	
32	Strain B	T658.1	CD220_i5_A	Input	98.7	7247386	N/A	
33	Strain B	T658.1	CD529_i11_A	Input	98.9	8477778	N/A	
34	Strain B	T658.1	CD594_i27_A	Input	98.8	9366140	N/A	
35	Strain B::chd1Δ	T709.3h	CD182_i20_A	H3K9me3	97.3	10597328	CD180_i18_A	
36	Strain B::chd1Δ	T709.3h	CD441_i25_A	H3K9me3	97.7	10717376	CD439_i23_A	
37	Strain B::chd1Δ	T709.3h	CD181_i19_A	hH3	81.4	8090865	CD180_i18_A	
38	Strain B::chd1Δ	T709.3h	CD440_i24_A	hH3	99.0	9477493	CD439_i23_A	
39	Strain B::chd1Δ	T709.3h	CD180_i18_A	Input	98.6	8172534	N/A	
40	Strain B::chd1Δ	T709.3h	CD439_i23_A	Input	99.2	8324205	N/A	
41	Strain B::eri1Δ	T770.2h	CD240_i22_A	H3K9me3	96.5	8209183	CD238_i20_A	
42	Strain B::eri1Δ	T770.2h	CD431_i15_A	H3K9me3	97.5	9112162	CD429_i13_A	
43	Strain B::eri1Δ	T770.2h	CD430_i14_A	hH3	99.1	7200067	CD429_i13_A	
44	Strain B::eri1Δ	T770.2h	CD239_i21_A	hH3	98.3	7230932	CD238_i20_A	

* Number of aligned reads is reported for the nuclear genome (corresponding to the interval 64841-41123470 in *mNC12.lacO-tetO*)

Table S4. ChIP-seq libraries created and analyzed in this study (continued).

45	Strain B::eri1Δ	T770.2h	CD429_i13_A	Input	99.0	8010217	N/A	
46	Strain B::eri1Δ	T770.2h	CD238_i20_A	Input	98.7	10293198	N/A	
47	Strain B::flag−sad−6	T827.7h	CD528_i32_A	FLAG	37.1	4506548	CD527_i4_A	Bl
48	Strain B::flag−sad−6	T827.7h	CD763_i33_A	FLAG	98.5	10738768	CD672_i46_A	Bl
49	Strain B::flag−sad−6	T827.7h	CD764_i34_A	FLAG	96.6	9150853	CD672_i46_A	Bl
50	Strain B::flag−sad−6	T827.7h	CD765_i35_A	FLAG	97.1	10576241	CD677_i41_A	Bl+Tc
51	Strain B::flag−sad−6	T827.7h	CD766_i36_A	FLAG	98.0	12321810	CD677_i41_A	Bl+Tc
52	Strain B::flag−sad−6	T827.7h	CD675_i43_A	GFP	97.9	10072417	CD672_i46_A	Bl
53	Strain B::flag−sad−6	T827.7h	CD604_i39_A	GFP	97.3	10537132	CD601_i43_A	Bl+Tc
54	Strain B::flag−sad−6	T827.7h	CD680_i38_A	GFP	98.4	10691467	CD677_i41_A	Bl+Tc
55	Strain B::flag−sad−6	T827.7h	CD674_i44_A	H3K9me3	96.8	10377412	CD672_i46_A	Bl
56	Strain B::flag−sad−6	T827.7h	CD799_i38_A	H3K9me3	91.3	5666258	CD527_i4_A	Bl
57	Strain B::flag−sad−6	T827.7h	CD603_i40_A	H3K9me3	97.6	9444811	CD601_i43_A	Bl+Tc
58	Strain B::flag−sad−6	T827.7h	CD679_i39_A	H3K9me3	97.3	10487142	CD677_i41_A	Bl+Tc
59	Strain B::flag−sad−6	T827.7h	CD673_i45_A	hH3	98.6	10431332	CD672_i46_A	Bl
60	Strain B::flag−sad−6	T827.7h	CD798_i37_A	hH3	98.8	7057779	CD527_i4_A	Bl
61	Strain B::flag−sad−6	T827.7h	CD602_i41_A	hH3	98.8	10748400	CD601_i43_A	Bl+Tc
62	Strain B::flag−sad−6	T827.7h	CD678_i40_A	hH3	98.8	10514385	CD677_i41_A	Bl+Tc
63	Strain B::flag−sad−6	T827.7h	CD527_i4_A	Input	98.9	10730984	N/A	Bl
64	Strain B::flag−sad−6	T827.7h	CD672_i46_A	Input	98.8	11006000	N/A	Bl
65	Strain B::flag−sad−6	T827.7h	CD601_i43_A	Input	98.9	10390350	N/A	Bl+Tc
66	Strain B::flag−sad−6	T827.7h	CD677_i41_A	Input	98.8	11240383	N/A	Bl+Tc
67	Strain B::hda1Δ	T714.8h	CD138_i34_A	H3K9me3	96.8	5320153	CD136_i17_A	
68	Strain B::hda1Δ	T714.8h	CD137_i19_A	hH3	99.1	7581904	CD136_i17_A	
69	Strain B::hda1Δ	T714.8h	CD136_i17_A	Input	98.9	7478362	N/A	
70	Strain B::qde−1Δ	T710.2h	CD424_i1_A	GFP	97.2	8583286	CD421_i5_A	
71	Strain B::qde−1Δ	T710.2h	CD435_i19_A	GFP	93.1	7774689	CD432_i16_A	
72	Strain B::qde−1Δ	T710.2h	CD423_i7_A	H3K9me3	97.3	7300690	CD421_i5_A	
73	Strain B::qde−1Δ	T710.2h	CD434_i18_A	H3K9me3	97.2	8452778	CD432_i16_A	
74	Strain B::qde−1Δ	T710.2h	CD422_i6_A	hH3	99.0	8298992	CD421_i5_A	
75	Strain B::qde−1Δ	T710.2h	CD433_i17_A	hH3	98.9	9519976	CD432_i16_A	
76	Strain B::qde−1Δ	T710.2h	CD421_i5_A	Input	99.0	8638738	N/A	
77	Strain B::qde−1Δ	T710.2h	CD432_i16_A	Input	99.0	7704419	N/A	
78	Strain B::qde−2Δ	T711.21h	CD196_i32_A	H3K9me3	96.6	7747370	CD194_i30_A	
79	Strain B::qde−2Δ	T711.21h	CD438_i22_A	H3K9me3	97.0	8674141	CD436_i20_A	
80	Strain B::qde−2Δ	T711.21h	CD195_i31_A	hH3	98.5	8368280	CD194_i30_A	
81	Strain B::qde−2Δ	T711.21h	CD437_i21_A	hH3	69.3	6663839	CD436_i20_A	
82	Strain B::qde−2Δ	T711.21h	CD194_i30_A	Input	98.5	8488470	N/A	
83	Strain B::qde−2Δ	T711.21h	CD436_i20_A	Input	99.1	9493385	N/A	
84	Strain B::qde−3Δ	T712.2h	CD428_i12_A	GFP	97.8	6900465	CD425_i9_A	
85	Strain B::qde−3Δ	T712.2h	CD445_i29_A	GFP	98.6	6917632	CD442_i26_A	
86	Strain B::qde−3Δ	T712.2h	CD129_i44_A	H3K9me3	96.8	8243938	CD127_i43_A	
87	Strain B::qde−3Δ	T712.2h	CD444_i28_A	H3K9me3	97.2	8428380	CD442_i26_A	
88	Strain B::qde−3Δ	T712.2h	CD427_i11_A	H3K9me3	97.4	6846737	CD425_i9_A	
89	Strain B::qde−3Δ	T712.2h	CD128_i15_A	hH3	98.8	7664057	CD127_i43_A	
90	Strain B::qde−3Δ	T712.2h	CD426_i10_A	hH3	99.1	7094939	CD425_i9_A	
91	Strain B::qde−3Δ	T712.2h	CD443_i27_A	hH3	97.3	8516563	CD442_i26_A	
92	Strain B::qde−3Δ	T712.2h	CD127_i43_A	Input	98.8	8261073	N/A	
93	Strain B::qde−3Δ	T712.2h	CD442_i26_A	Input	99.1	6015297	N/A	
94	Strain B::qde−3Δ	T712.2h	CD425_i9_A	Input	99.1	7512143	N/A	

Table S4. ChIP-seq libraries created and analyzed in this study (continued).

95	Strain B::rad51Δ	T737.1h	CD147_i41_A	H3K9me3	97.0	8337203	CD145_i39_A	
96	Strain B::rad51Δ	T737.1h	CD404_i24_A	H3K9me3	97.2	10136955	CD402_i22_A	
97	Strain B::rad51Δ	T737.1h	CD403_i23_A	hH3	99.0	9258535	CD402_i22_A	
98	Strain B::rad51Δ	T737.1h	CD762_i32_A	hH3	98.4	8957878	CD145_i39_A	
99	Strain B::rad51Δ	T737.1h	CD145_i39_A	Input	97.8	8378515	N/A	
100	Strain B::rad51Δ	T737.1h	CD402_i22_A	Input	98.9	9409013	N/A	
101	Strain B::rad52Δ	T738.1h	CD186_i24_A	H3K9me3	96.5	9324486	CD184_i22_A	
102	Strain B::rad52Δ	T738.1h	CD407_i27_A	H3K9me3	97.1	9284593	CD405_i25_A	
103	Strain B::rad52Δ	T738.1h	CD185_i23_A	hH3	98.5	8814243	CD184_i22_A	
104	Strain B::rad52Δ	T738.1h	CD406_i26_A	hH3	99.0	8800775	CD405_i25_A	
105	Strain B::rad52Δ	T738.1h	CD184_i22_A	Input	98.5	9206043	N/A	
106	Strain B::rad52Δ	T738.1h	CD405_i25_A	Input	99.0	9393715	N/A	
107	Strain B::rtt109Δ	T786.3h	CD377_i48_A	H3K9me3	95.6	6482608	CD375_i47_A	
108	Strain B::rtt109Δ	T786.3h	CD448_i32_A	H3K9me3	97.2	7149877	CD446_i30_A	
109	Strain B::rtt109Δ	T786.3h	CD376_i29_A	hH3	98.3	8275565	CD375_i47_A	
110	Strain B::rtt109Δ	T786.3h	CD447_i31_A	hH3	99.0	7456714	CD446_i30_A	
111	Strain B::rtt109Δ	T786.3h	CD375_i47_A	Input	98.7	7137760	N/A	
112	Strain B::rtt109Δ	T786.3h	CD446_i30_A	Input	99.1	7804782	N/A	
113	Strain B::sad−6Δ	T707.51h	CD458_i42_A	GFP	98.5	9891388	CD454_i38_A	Tc
114	Strain B::sad−6Δ	T707.51h	CD632_i6_A	GFP	98.8	8444453	CD629_i9_A	Tc
115	Strain B::sad−6Δ	T707.51h	CD262_i43_A	GFP	93.1	7346354	CD259_i40_A	
116	Strain B::sad−6Δ	T707.51h	CD401_i21_A	GFP	98.2	8513589	CD398_i18_A	
117	Strain B::sad−6Δ	T707.51h	CD456_i40_A	H3K9me3	98.1	10193635	CD454_i38_A	Tc
118	Strain B::sad−6Δ	T707.51h	CD631_i7_A	H3K9me3	97.4	9147582	CD629_i9_A	Tc
119	Strain B::sad−6Δ	T707.51h	CD261_i42_A	H3K9me3	97.0	8832346	CD259_i40_A	
120	Strain B::sad−6Δ	T707.51h	CD400_i20_A	H3K9me3	97.0	7928262	CD398_i18_A	
121	Strain B::sad−6Δ	T707.51h	CD736_i31_A	hH2B	99.0	8931671	CD454_i38_A	Tc
122	Strain B::sad−6Δ	T707.51h	CD737_i32_A	hH2B	98.9	7844732	CD629_i9_A	Tc
123	Strain B::sad−6Δ	T707.51h	CD733_i28_A	hH2B	98.9	9741353	CD398_i18_A	
124	Strain B::sad−6Δ	T707.51h	CD735_i30_A	hH2B	98.8	9109414	CD734_i29_A	
125	Strain B::sad−6Δ	T707.51h	CD455_i39_A	hH3	99.0	13205725	CD454_i38_A	Tc
126	Strain B::sad−6Δ	T707.51h	CD630_i8_A	hH3	98.8	9219792	CD629_i9_A	Tc
127	Strain B::sad−6Δ	T707.51h	CD260_i41_A	hH3	98.5	7870943	CD259_i40_A	
128	Strain B::sad−6Δ	T707.51h	CD399_i19_A	hH3	98.9	9548072	CD398_i18_A	
129	Strain B::sad−6Δ	T707.51h	CD454_i38_A	Input	99.2	11323585	N/A	Tc
130	Strain B::sad−6Δ	T707.51h	CD629_i9_A	Input	99.0	9775144	N/A	Tc
131	Strain B::sad−6Δ	T707.51h	CD259_i40_A	Input	98.8	12084203	N/A	
132	Strain B::sad−6Δ	T707.51h	CD398_i18_A	Input	99.0	10727138	N/A	
133	Strain B::sad−6Δ	T707.51h	CD734_i29_A	Input	98.8	8947082	N/A	
134	Strain C	C290.6	CD69_i37_A	H3K9me3	98.4	7002290	CD67_i35_A	
135	Strain C	C290.6	CD569_i45_A	H3K9me3	95.3	7793367	CD567_i48_A	
136	Strain C	C290.6	CD68_i36_A	hH3	98.8	8373074	CD67_i35_A	
137	Strain C	C290.6	CD568_i46_A	hH3	98.4	7145823	CD567_i48_A	
138	Strain C	C290.6	CD67_i35_A	Input	98.4	8426641	N/A	
139	Strain C	C290.6	CD567_i48_A	Input	98.5	8075101	N/A	
140	Strain C::lacO(d1); dim−5+	T697.1	CD61_i48_A	H3K9me3	97.8	5278648	CD60_i47_A	
141	Strain C::lacO(d1); dim−5+	T697.1	CD556_i36_A	H3K9me3	96.7	8153045	CD555_i37_A	
142	Strain C::lacO(d1); dim−5+	T697.1	CD60_i47_A	Input	99.3	6408038	N/A	
143	Strain C::lacO(d1); dim−5+	T697.1	CD555_i37_A	Input	99.0	9482890	N/A	
144	Strain C::lacO(d2); dim−5+	T698.1	CD66_i34_A	H3K9me3	88.5	7339481	CD65_i33_A	

Table S4. ChIP-seq libraries created and analyzed in this study (continued).

145	Strain C::lacO(d2); dim−5+	T698.1	CD558_i34_A	H3K9me3	96.5	6864519	CD557_i35_A	
146	Strain C::lacO(d2); dim−5+	T698.1	CD65_i33_A	Input	99.4	8631930	N/A	
147	Strain C::lacO(d2); dim−5+	T698.1	CD557_i35_A	Input	98.9	8147564	N/A	
148	Strain C::dim−5+	T663.2	CD40_i27_A	H3K9me3	97.8	10427164	CD38_i25_A	
149	Strain C::dim−5+	T663.2	CD769_i38_A	H3K9me3	95.0	9142215	CD294_i25_A	
150	Strain C::dim−5+	T663.2	CD39_i26_A	hH3	99.0	7942226	CD38_i25_A	
151	Strain C::dim−5+	T663.2	CD768_i37_A	hH3	98.9	10418247	CD294_i25_A	
152	Strain C::dim−5+	T663.2	CD38_i25_A	Input	99.2	6976064	N/A	
153	Strain C::dim−5+	T663.2	CD294_i25_A	Input	98.4	9361089	N/A	
154	Strain C::sad−6Δ	T752.13h	CD830_i29_A	hH3	98.7	8808509	CD829_i28_A	
155	Strain C::sad−6Δ	T752.13h	CD829_i28_A	Input	98.7	10053671	N/A	
156	Strain D::chapΔ	T690.1h	CD49_i36_A	H3K9me3	97.5	9337383	CD47_i34_A	
157	Strain D::chapΔ	T690.1h	CD579_i33_A	H3K9me3	97.2	8135547	CD577_i35_A	
158	Strain D::chapΔ	T690.1h	CD48_i35_A	hH3	99.2	8855879	CD47_i34_A	
159	Strain D::chapΔ	T690.1h	CD578_i34_A	hH3	98.6	7111554	CD577_i35_A	
160	Strain D::chapΔ	T690.1h	CD47_i34_A	Input	99.1	6600607	N/A	
161	Strain D::chapΔ	T690.1h	CD577_i35_A	Input	92.5	7972673	N/A	
162	Strain D::dim−7Δ	T688.2h	CD43_i30_A	H3K9me3	98.3	6777728	CD41_i28_A	
163	Strain D::dim−7Δ	T688.2h	CD573_i40_A	H3K9me3	94.2	8595604	CD571_i43_A	
164	Strain D::dim−7Δ	T688.2h	CD42_i29_A	hH3	99.2	11718495	CD41_i28_A	
165	Strain D::dim−7Δ	T688.2h	CD572_i41_A	hH3	98.5	7047100	CD571_i43_A	
166	Strain D::dim−7Δ	T688.2h	CD41_i28_A	Input	99.1	8792743	N/A	
167	Strain D::dim−7Δ	T688.2h	CD571_i43_A	Input	98.6	8428865	N/A	
168	Strain D::dim−9Δ	T689.2h	CD46_i33_A	H3K9me3	98.4	8255276	CD44_i31_A	
169	Strain D::dim−9Δ	T689.2h	CD576_i36_A	H3K9me3	96.9	9271303	CD574_i39_A	
170	Strain D::dim−9Δ	T689.2h	CD45_i32_A	hH3	99.2	9513255	CD44_i31_A	
171	Strain D::dim−9Δ	T689.2h	CD575_i38_A	hH3	98.8	9986908	CD574_i39_A	
172	Strain D::dim−9Δ	T689.2h	CD44_i31_A	Input	99.2	6616746	N/A	
173	Strain D::dim−9Δ	T689.2h	CD574_i39_A	Input	98.5	10005228	N/A	
174	Strain D::hda1Δ	T743.3h	CD135_i48_A	H3K9me3	97.1	6833539	CD133_i47_A	
175	Strain D::hda1Δ	T743.3h	CD134_i18_A	hH3	98.9	8831960	CD133_i47_A	
176	Strain D::hda1Δ	T743.3h	CD133_i47_A	Input	98.9	6330925	N/A	
177	Strain E	T601.2h	CD848_i36_A	H3K9me3	93.7	8643593	CD845_i33_A	"maintained"
178	Strain E	T601.2h	CD844_i42_A	H3K9me3	96.6	7761265	CD843_i41_A	"released"
179	Strain E	T601.2h	CD852_i4_A	H3K9me3	92.3	8634000	CD849_i1_A	"released"
180	Strain E	T601.2h	CD655_i37_A	H3K9me3	98.1	8476509	CD653_i35_A	no-N
181	Strain E	T601.2h	CD750_i25_A	H3K9me3	97.4	8908047	CD723_i18_A	no-N
182	Strain E	T601.2h	CD75_i43_A	H3K9me3	97.5	7793876	CD73_i41_A	
183	Strain E	T601.2h	CD652_i34_A	H3K9me3	98.5	8145259	CD650_i32_A	
184	Strain E	T601.2h	CD741_i36_A	hH2B	98.8	10530685	CD723_i18_A	no-N
185	Strain E	T601.2h	CD740_i35_A	hH2B	98.9	8585096	CD697_i24_A	no-N
186	Strain E	T601.2h	CD738_i33_A	hH2B	98.8	9637627	CD650_i32_A	
187	Strain E	T601.2h	CD739_i34_A	hH2B	99.0	8700628	CD721_i16_A	
188	Strain E	T601.2h	CD654_i36_A	hH3	96.3	7792030	CD653_i35_A	no-N
189	Strain E	T601.2h	CD698_i23_A	hH3	98.6	8852422	CD697_i24_A	no-N
190	Strain E	T601.2h	CD74_i42_A	hH3	99.1	8816753	CD73_i41_A	
191	Strain E	T601.2h	CD651_i33_A	hH3	99.1	8817367	CD650_i32_A	
192	Strain E	T601.2h	CD845_i33_A	Input	99.1	9926094	N/A	"maintained"
193	Strain E	T601.2h	CD843_i41_A	Input	98.9	9427679	N/A	"released"
194	Strain E	T601.2h	CD849_i1_A	Input	99.0	9054557	N/A	"released"

Table S4. ChIP-seq libraries created and analyzed in this study (continued).

195	Strain E	T601.2h	CD723_i18_A	Input	99.0	9226469	N/A	no-N
196	Strain E	T601.2h	CD697_i24_A	Input	99.0	8445763	N/A	no-N
197	Strain E	T601.2h	CD653_i35_A	Input	99.0	9196543	N/A	no-N
198	Strain E	T601.2h	CD650_i32_A	Input	98.6	9355163	N/A	
199	Strain E	T601.2h	CD721_i16_A	Input	98.9	11369712	N/A	
200	Strain E	T601.2h	CD73_i41_A	Input	98.0	9209709	N/A	
201	Strain E::tetR−gfp	T753.1	CD190_i28_A	H3K9me3	96.8	8798934	CD188_i26_A	
202	Strain E::tetR−gfp	T753.1	CD614_i30_A	H3K9me3	97.4	7039957	CD612_i32_A	
203	Strain E::tetR−gfp	T753.1	CD189_i27_A	hH3	98.5	8198700	CD188_i26_A	
204	Strain E::tetR−gfp	T753.1	CD613_i31_A	hH3	99.0	9640803	CD612_i32_A	
205	Strain E::tetR−gfp	T753.1	CD188_i26_A	Input	98.6	7988786	N/A	
206	Strain E::tetR−gfp	T753.1	CD612_i32_A	Input	98.9	11275351	N/A	
207	Strain E::nit−2Δ	T851.1h	CD667_i48_A	H3K9me3	98.4	8032158	CD665_i46_A	no-N
208	Strain E::nit−2Δ	T851.1h	CD690_i28_A	H3K9me3	96.3	9369072	CD688_i30_A	no-N
209	Strain E::nit−2Δ	T851.1h	CD666_i47_A	hH3	98.4	9158422	CD665_i46_A	no-N
210	Strain E::nit−2Δ	T851.1h	CD689_i29_A	hH3	98.4	9083438	CD688_i30_A	no-N
211	Strain E::nit−2Δ	T851.1h	CD665_i46_A	Input	99.1	10457276	N/A	no-N
212	Strain E::nit−2Δ	T851.1h	CD688_i30_A	Input	98.9	9823600	N/A	no-N
213	Strain E::qde−1Δ	T839.10h	CD608_i35_A	H3K9me3	88.5	10022605	CD606_i36_A	no-N
214	Strain E::qde−1Δ	T839.10h	CD711_i6_A	H3K9me3	98.2	6636860	CD709_i4_A	no-N
215	Strain E::qde−1Δ	T839.10h	CD607_i27_A	hH3	98.6	9631010	CD606_i36_A	no-N
216	Strain E::qde−1Δ	T839.10h	CD710_i5_A	hH3	98.8	8712589	CD709_i4_A	no-N
217	Strain E::qde−1Δ	T839.10h	CD606_i36_A	Input	98.9	12868225	N/A	no-N
218	Strain E::qde−1Δ	T839.10h	CD709_i4_A	Input	99.2	8851401	N/A	no-N
219	Strain E::qde−3Δ	T840.10h	CD611_i33_A	H3K9me3	97.7	10392870	CD609_i34_A	no-N
220	Strain E::qde−3Δ	T840.10h	CD752_i26_A	H3K9me3	97.7	9109045	CD715_i10_A	no-N
221	Strain E::qde−3Δ	T840.10h	CD610_i26_A	hH3	86.9	7683121	CD609_i34_A	no-N
222	Strain E::qde−3Δ	T840.10h	CD716_i11_A	hH3	99.0	7553969	CD715_i10_A	no-N
223	Strain E::qde−3Δ	T840.10h	CD715_i10_A	Input	99.2	9094349	N/A	no-N
224	Strain E::qde−3Δ	T840.10h	CD609_i34_A	Input	99.1	10277658	N/A	no-N
225	Strain E::rad51Δ	T847.3h	CD708_i3_A	H3K9me3	77.4	5436037	CD706_i1_A	no-N
226	Strain E::rad51Δ	T847.3h	CD754_i27_A	H3K9me3	97.8	8943634	CD700_i21_A	no-N
227	Strain E::rad51Δ	T847.3h	CD701_i20_A	hH3	99.0	9300497	CD700_i21_A	no-N
228	Strain E::rad51Δ	T847.3h	CD707_i2_A	hH3	97.7	8549931	CD706_i1_A	no-N
229	Strain E::rad51Δ	T847.3h	CD700_i21_A	Input	99.0	10417937	N/A	no-N
230	Strain E::rad51Δ	T847.3h	CD706_i1_A	Input	99.1	7828349	N/A	no-N
231	Strain E::rad52Δ	T848.1h	CD714_i9_A	H3K9me3	97.0	7071655	CD712_i7_A	no-N
232	Strain E::rad52Δ	T848.1h	CD756_i28_A	H3K9me3	97.7	9872070	CD703_i18_A	no-N
233	Strain E::rad52Δ	T848.1h	CD704_i17_A	hH3	98.5	9440003	CD703_i18_A	no-N
234	Strain E::rad52Δ	T848.1h	CD713_i8_A	hH3	98.8	7385596	CD712_i7_A	no-N
235	Strain E::rad52Δ	T848.1h	CD703_i18_A	Input	99.0	8137387	N/A	no-N
236	Strain E::rad52Δ	T848.1h	CD712_i7_A	Input	99.0	8000728	N/A	no-N
237	Strain E::sad−6Δ	T774.4h	CD658_i40_A	H3K9me3	97.7	9927567	CD656_i38_A	no-N
238	Strain E::sad−6Δ	T774.4h	CD687_i31_A	H3K9me3	96.5	9708825	CD685_i33_A	no-N
239	Strain E::sad−6Δ	T774.4h	CD745_i40_A	hH2B	98.9	7706122	CD685_i33_A	no-N
240	Strain E::sad−6Δ	T774.4h	CD746_i41_A	hH2B	98.7	7986318	CD727_i22_A	no-N
241	Strain E::sad−6Δ	T774.4h	CD742_i37_A	hH2B	99.0	10163595	CD725_i20_A	
242	Strain E::sad−6Δ	T774.4h	CD744_i39_A	hH2B	98.8	9149919	CD743_i38_A	
243	Strain E::sad−6Δ	T774.4h	CD657_i39_A	hH3	98.5	9787164	CD656_i38_A	no-N
244	Strain E::sad−6Δ	T774.4h	CD686_i32_A	hH3	98.5	9187849	CD685_i33_A	no-N

Table S4. ChIP-seq libraries created and analyzed in this study (continued).

245	Strain E::sad−6Δ	T774.4h	CD685_i33_A	Input	98.9	8575543	N/A	no-N
246	Strain E::sad−6Δ	T774.4h	CD656_i38_A	Input	99.0	9538401	N/A	no-N
247	Strain E::sad−6Δ	T774.4h	CD727_i22_A	Input	99.0	8307630	N/A	no-N
248	Strain E::sad−6Δ	T774.4h	CD725_i20_A	Input	98.9	9546376	N/A	
249	Strain E::sad−6Δ	T774.4h	CD743_i38_A	Input	98.4	9014884	N/A	
250	Strain F::lacO(i1); dim−5+	T764.1	CD202_i38_A	H3K9me3	96.9	7305893	CD201_i37_A	
251	Strain F::lacO(i1); dim−5+	T764.1	CD562_i30_A	H3K9me3	96.8	9060889	CD561_i31_A	
252	Strain F::lacO(i1); dim−5+	T764.1	CD201_i37_A	Input	98.5	6529896	N/A	
253	Strain F::lacO(i1); dim−5+	T764.1	CD561_i31_A	Input	98.8	10258869	N/A	
254	Strain F::lacO(i2); dim−5+	T766.1	CD204_i40_A	H3K9me3	96.1	5680629	CD203_i39_A	
255	Strain F::lacO(i2); dim−5+	T766.1	CD564_i28_A	H3K9me3	96.6	8147239	CD563_i29_A	
256	Strain F::lacO(i2); dim−5+	T766.1	CD203_i39_A	Input	98.4	8587633	N/A	
257	Strain F::lacO(i2); dim−5+	T766.1	CD563_i29_A	Input	98.5	8521230	N/A	
258	Strain F::lacO(i3); dim−5+	T776.1	CD206_i42_A	H3K9me3	96.7	6528076	CD205_i41_A	
259	Strain F::lacO(i3); dim−5+	T776.1	CD566_i42_A	H3K9me3	97.2	7423559	CD565_i47_A	
260	Strain F::lacO(i3); dim−5+	T776.1	CD205_i41_A	Input	98.6	5535835	N/A	
261	Strain F::lacO(i3); dim−5+	T776.1	CD565_i47_A	Input	98.9	8428602	N/A	

Table S5. MNase-seq libraries created and analyzed in this study.

#	Genetic condition	Strain ID	Library	Alignment rate (%)	Aligned reads *	Additional conditions
1	Strain A	T647.1h	CD1072_i0_A	99.3	26796362	
2	Strain B	T658.1	CD530_i12_A	99.1	10769647	
3	Strain B::sad−6Δ	T707.51h	CD533_i15_A	99.0	12371585	
4	Strain C	C290.6	CD290_i21_A	98.5	11797272	
5	Strain C::sad−6Δ	T752.13h	CD832_i30_A	99.2	12764340	
6	Strain E	T601.2h	CD722_i17_A	99.1	11456746	
7	Strain E	T601.2h	CD587_i15_A	99.2	15232062	no-N
8	Strain E::sad−6Δ	T774.4h	CD589_i14_A	99.3	14815243	no-N

* Number of aligned reads is reported for the nuclear genome (corresponding to the interval 64841-41123470 in *mNC12.lacO-tetO*)

Table S6. sRNA-seq libraries created and analyzed in this study.

#	Genetic condition	Strain ID	Library	Alignment rate (%)	Mitochondrial reads	Ribosomal reads	Core nuclear reads	Additional conditions
1	Strain A	T647.1h	VR18_i16_A	91.5	89140	6334645	768640	
2	Strain A	T647.1h	VR167_i2_A	94.5	273129	4821765	1112917	
3	Strain B	T658.1	VR13_i11_A	94.7	72864	3349707	669524	
4	Strain B	T658.1	VR200_i19_A	95.1	354937	6246084	2046200	
5	Strain B	T658.1	VR259_i47_A	92.6	330465	4767444	1953046	Bl
6	Strain B	T658.1	VR274_i37_A	95.3	397237	6514549	2298582	Bl
7	Strain B	T658.1	VR48_i25_A	93.6	1591285	3207673	923786	HU
8	Strain B	T658.1	VR202_i21_A	94.3	1523622	4343824	2032401	HU
9	Strain B	T658.1	VR201_i20_A	95.9	283061	6067766	1137260	Tc
10	Strain B	T658.1	VR232_i43_A	95.0	100545	7477216	1011309	Tc
11	Strain B::chd1Δ	T709.3h	VR181_i9_A	95.1	365062	5327883	2700055	
12	Strain B::chd1Δ	T709.3h	VR234_i45_A	95.0	228614	4714202	1942622	
13	Strain B::eri1Δ	T770.2h	VR156_i18_A	93.7	208510	3976531	2827441	
14	Strain B::eri1Δ	T770.2h	VR226_i43_A	94.6	168717	5107627	2397763	
15	Strain B::flag−sad−6	T827.7h	VR275_i38_A	95.2	362259	6686193	1841027	Bl
16	Strain B::flag−sad−6	T827.7h	VR328_i0_A	86.5	140179	4821635	969352	Bl
17	Strain B::hda1Δ	T714.8h	VR67_i20_A	96.4	117222	1653395	4463222	
18	Strain B::hda1Δ	T714.8h	VR187_i5_A	93.3	180826	2141171	5662706	
19	Strain B::qde−1Δ	T710.2h	VR51_i28_A	94.1	199541	5057507	1055664	
20	Strain B::qde−1Δ	T710.2h	VR158_i20_A	93.8	337753	5208452	1259318	
21	Strain B::qde−2Δ	T711.21h	VR159_i21_A	91.0	176974	3485602	2274100	
22	Strain B::qde−2Δ	T711.21h	VR206_i25_A	90.5	352184	6498566	3417528	
23	Strain B::qde−3Δ	T712.2h	VR75_i33_A	96.0	175742	4122871	622478	
24	Strain B::qde−3Δ	T712.2h	VR207_i26_A	90.3	177939	5426733	786112	
25	Strain B::rad51Δ	T737.1h	VR182_i46_A	94.9	272390	5804726	3582359	
26	Strain B::rad51Δ	T737.1h	VR219_i36_A	93.3	285179	7066045	2967365	
27	Strain B::rad52Δ	T738.1h	VR178_i42_A	95.2	234040	3694120	7134007	
28	Strain B::rad52Δ	T738.1h	VR210_i29_A	94.0	213286	3682292	4382441	
29	Strain B::rtt109Δ	T786.3h	VR213_i32_A	94.0	127733	6865730	1343029	
30	Strain B::rtt109Δ	T786.3h	VR221_i38_A	94.4	171898	6281191	1998765	
31	Strain B::sad−6Δ	T707.51h	VR157_i19_A	92.4	384973	5419815	1623912	
32	Strain B::sad−6Δ	T707.51h	VR204_i23_A	95.4	305828	5999418	905752	
33	Strain B::top3Δ	T812.11h	VR242_i42_A	95.8	175430	3631633	4186739	
34	Strain B::top3Δ	T812.11h	VR246_i46_A	94.8	122062	5173798	2023411	
35	Strain C	C290.6	VR139_i1_A	94.0	270021	5810093	2915944	
36	Strain C	C290.6	VR195_i14_A	90.4	192356	3984691	2252637	
37	Strain C	C290.6	VR15_i13_A	88.9	598556	2738413	756356	HU
38	Strain C	C290.6	VR199_i18_A	93.8	296056	5583631	1021777	HU
39	Strain C::lacO(d1)	C290.6.C4	VR4_i3_A	95.4	101949	3745549	961248	
40	Strain C::lacO(d1)	C290.6.C4	VR264_i27_A	96.5	248698	6752046	2180782	
41	Strain C::lacO(d2)	C290.6.C6	VR5_i28_A	92.3	124222	3910687	1078488	
42	Strain C::lacO(d2)	C290.6.C6	VR265_i28_A	93.8	334516	6952769	3550683	
43	Strain C::dim−5+	T663.2	VR1_i27_A	96.3	176973	5096301	894206	
44	Strain C::dim−5+	T663.2	VR140_i2_A	95.2	323739	9390098	1655988	

Table S6. sRNA-seq libraries created and analyzed in this study (continued).

45	Strain C::qde−1Δ	T739.4h	VR52_i29_A	96.3	167825	5736656	849642	
46	Strain C::qde−1Δ	T739.4h	VR170_i34_A	94.6	63998	8986893	962974	
47	Strain C::qde−1Δ	T739.4h	VR368_i2_A	97.9	254400	22662127	2471385	
48	Strain C::rad51Δ	T678.5h	VR27_i23_A	95.2	186305	6174654	2362345	
49	Strain C::rad51Δ	T678.5h	VR41_i18_A	90.0	62074	2358548	1006793	
50	Strain C::rad51Δ	T678.5h	VR177_i41_A	94.3	215374	4479746	5634639	
51	Strain C::sad−6Δ	T752.13h	VR255_i39_A	96.1	153384	9522494	1376775	
52	Strain C::sad−6Δ	T752.13h	VR260_i48_A	95.9	143268	7577198	1006200	
53	Strain D::chapΔ	T690.1h	VR186_i26_A	91.5	830143	4924184	2136729	
54	Strain D::chapΔ	T690.1h	VR198_i17_A	94.7	166768	5612364	1034516	
55	Strain D::dim−7Δ	T688.2h	VR6_i4_A	96.5	161363	5416165	1501359	
56	Strain D::dim−7Δ	T688.2h	VR143_i5_A	94.2	185216	7371866	2690269	
57	Strain D::dim−9Δ	T689.2h	VR7_i5_A	95.5	119282	3553738	1260019	
58	Strain D::dim−9Δ	T689.2h	VR266_i29_A	95.3	225356	7131021	2355417	
59	Strain D::hda1Δ	T743.3h	VR62_i13_A	94.1	85391	1872060	2123860	
60	Strain D::hda1Δ	T743.3h	VR179_i43_A	93.4	209183	4538707	4005878	
61	Strain E	T601.2h	VR166_i30_A	94.5	435793	6926994	1351635	
62	Strain E	T601.2h	VR347_i0_A	93.0	304726	12151367	1691174	
63	Strain E	T601.2h	VR304_i23_A	95.2	312596	7185662	2676606	no-N
64	Strain E	T601.2h	VR308_i1_A	94.5	384311	6889801	1990153	no-N
65	Strain E	T601.2h	VR280_i43_A	94.3	176832	4934667	894476	N+ control
66	Strain E	T601.2h	VR350_i48_A	93.8	46571	4022817	559369	N+ control
67	Strain E	T601.2h	VR353_i46_A	94.2	134854	5476783	813063	N+ control
68	Strain E	T601.2h	VR314_i7_A	94.3	678899	9254058	1398482	"released"
69	Strain E	T601.2h	VR315_i8_A	94.0	330082	7129312	1850101	"maintained"
70	Strain E::tetR−gfp	T753.1	VR180_i44_A	89.2	231596	8574884	2001104	
71	Strain E::tetR−gfp	T753.1	VR208_i27_A	93.8	256389	6289769	2410247	
72	Strain E::nit−2Δ	T851.1h	VR329_i0_A	93.2	290039	8427720	1701623	no-N
73	Strain E::nit−2Δ	T851.1h	VR330_i0_A	94.5	250838	8409414	1660895	no-N
74	Strain E::nit−2Δ	T851.1h	VR344_i5_A	95.4	194513	6910524	1270996	no-N
75	Strain E::qde−1Δ	T839.10h	VR312_i0_A	95.4	889847	17261386	2543135	no-N
76	Strain E::qde−1Δ	T839.10h	VR316_i0_A	95.1	521087	11517703	1726187	no-N
77	Strain E::qde−3Δ	T840.10h	VR313_i0_A	95.1	917304	16945619	2790338	no-N
78	Strain E::qde−3Δ	T840.10h	VR317_i0_A	95.2	746121	12363669	2086566	no-N
79	Strain E::rad51Δ	T847.3h	VR331_i3_B	94.2	181149	3410221	2840787	no-N
80	Strain E::rad51Δ	T847.3h	VR332_i4_C	94.3	245869	5105236	4387030	no-N
81	Strain E::rad52Δ	T848.1h	VR333_i5_B	92.9	129785	3427957	2487608	no-N
82	Strain E::rad52Δ	T848.1h	VR334_i6_B	90.7	103778	3446758	1789739	no-N
83	Strain E::sad−6Δ	T774.4h	VR302_i0_A	94.6	397546	10630045	1666933	no-N
84	Strain E::sad−6Δ	T774.4h	VR348_i0_A	95.0	431348	12883573	2143730	no-N
85	Strain F::lacO(i1)	T724.2h	VR76_i4_A	91.1	121473	3805143	899079	
86	Strain F::lacO(i1)	T724.2h	VR189_i7_A	90.8	272686	3757672	2319565	
87	Strain F::lacO(i2)	T726.1h	VR80_i8_A	93.5	132936	3561318	1139354	
88	Strain F::lacO(i2)	T726.1h	VR191_i10_A	91.8	467307	4934028	2998980	
89	Strain F::lacO(i3)	T728.1h	VR81_i25_A	85.6	62911	3848337	583177	